The Milky Way's merger history analyzed via high-resolution hydrodynamical simulations

Milan Quandt Rodríguez

Tutors: Arianna Di Cintio & Christopher Brook

Master's degree in Astrophysics
ULL 2022-2023

Abstract

Desde hace más de una decada se conocen importantes discrepancias entre lo que el modelo actual de formación de galaxias y más en general, el modelo cosmológico actual ΛCDM espera, y lo que muestran las observaciones. Estas discrepancias se acentúan sobre todo en galaxias más pequeñas, catalogadas normalmente como galaxias con masas estelares menores a 10^9 masas solares y bautizadas como galaxias enanas (del inglés *dwarf galaxies*). Ocurre por un lado, que las galaxias satélite, es decir, las que orbitan otras galaxias más masivas en nuestro Grupo Local, parecen estar alineadas en planos de rotación en lugar de estar distribuidas de manera aleatoria. Además de eso, cuando se hacen las cuentas de las galaxias satélite observadas frente a las simuladas en simulaciones cosmológicas, hay una importante discrepancia en el número a favor de las simuladas. Últimamente se ha aliviado esta discrepancia por dos motivos principales: el aumento del límite instrumental de detección de brillo, el cual ha permitido la detección de galaxias muy poco brillantes hasta la fecha desconocidas por un lado, y la inclusión de materia bariónica y *feedback* en las simulaciones, con lo que se consigue reducir el número de satélites por otro.

Una tercera mejora sustancial viene dada por el hecho de tener en cuenta el particular mapa cosmográfico de nuestro Grupo Local al simularlo. Esta es quizás la mayor particularidad de las simulaciones hidrodinámicas HESTIA, las cuales "fuerzan" sus Vías Lácteas simuladas a vivir en un entorno espacial de 3 Mpc como el que las observaciones cosmográficas de hoy en día indican. Haciendo uso de las 24 simulaciones de media resolución y 3 simulacines de alta resolución HESTIA, dividimos nuestro trabajo en dos partes: En una primera parte, tratamos de seleccionar de entre las 24 candidatas (más las tres de alta resolución) la que mejor se adhiere a las observaciones conocidas hasta la fecha, filtrando las diferentes candidatas bien por morfología y bien por historia de formación estelar y historia de acreción de masa. Estas dos últimas características están íntimamente ligadas al principal evento de acreción de nuestra Vía Láctea acaecido hace unos 10 gigaaños, el cual propulsó la formación de estrellas drásticamente, a la vez que al incluir estrellas de la galaxia acretada entre las suyas propias, formó una segunda secuencia principal con estrellas de menor metalicidad y distinta cinemática. El objetivo principal de la selección de una Vía Láctea que represente de forma más fiel lo que conocemos sobre ella a día de hoy, es obtener un conjunto de condiciones iniciales para correr simulaciones en el futuro. Después de aplicar los filtros recién mencionados, seleccionamos la simulación de alta resolución 37_11 como mejor candidata.

La segunda parte del trabajo se centra en las galaxias satélite de las dos principales galaxias de cada uno de los 3 grupos locales simulados en alta resolución 09_18, 17_11 y 37_11. En particular, se trata de dar respuesta a una serie de preguntas que nos planteamos con ánimo de arrojar algo de luz sobre algunos de los problemas que forman parte de la llamada crisis a pequeña escala (*small-scale crisis*) del modelo cosmológico actual. Para comenzar identificamos todas las galaxias satélite en cada una de las principales galaxias como halos incluidas en el radio del virial con masas estelares mayores a 10^6 masas solares. Además de ello, es necesario establecer un filtro adicional, y es que para asegurar la suficiente presencia de materia oscura en cada halo, el ratio de materia bariónica frente a materia oscura sea menor a 0.1. Una vez identificadas, se obtienen las masas, la posición y cinemática de cada una de ellas. Se observan 3 candidatas con una posible estructura planar, aunque no definitiva, debido a que ni es muy clara en el sentido del grosor del plano, ni se observa semejanza en la cinemática de las galaxias que la conforman. Ello nos hace pensar que se trata de estructuras más bien transitoras. Con lo que respecta a la cinemática de las galaxias, se obtiene el ratio de órbitas prógradas y retrógradas en el plano de rotación de los discos galácticos. Se obtiene un total de 22 galaxias prógradas frente a 24 retrógradas, lo cual no indica una particular preferencia por ninguno de los dos tipos de órbita. Una vez identificadas las galaxias y sus propiedades, se determinan sus tiempos de captación, el cual definimos como el instante en el cual la galaxia satélite cruzó por primera vez el radio del virial de su anfitriona y en lo sucesivo denotaremos como t_{infall}. La mayoría de las satélites son atraídas por primera vez a las inmediaciones de sus anfitrionas en los primeros 2-6 giga años de simulación. Únicamente 3 galaxias son atraídas en los últimos 2 giga años. No parace haber ninguna correlación entre el tiempo de primera caída de las galaxias satélite sobre las anfitrionas con el tipo de órbita. Al trazar la evolución espacial de las satélites a través de los diferentes *snaphots* observamos un fenómeno que parece ser común: 4 de las 6 galaxias anfitrionas estudiadas muestran una caída grupal de sus satélites. El 43% de las galaxias son captadas de manera grupal. En estas 4 están a la vez incluidas las 3 comentadas anteriormente con potenciales discos. Esta posible relación debe ser estudiada con más detenimiento debido al bajo número de galaxias estudiadas y la ambigüedad de las estructuras planares de las que hablamos. Podría ampliarse el estudio a las simulaciones de media resolución. Un segundo fenómeno común es el de las galaxias *backsplash*, en otras palabras galaxias que "rebotan" para volver a salir al menos una vez del radio del virial. 14/46 sufren este fenómeno. Finalmente, reproducimos la función de luminosidad tanto de la Vía Láctea como de M31. En dos de los casos, tanto en 09_18 como en 17_11 el resultado está dentro de lo esperado por las observaciones en el rango de baja luminosidad ($M_V > -12$), lo cual indica que este tipo de simulaciones sí resuleven el problema de "satélites perdidos". En el caso de 37_11, la simulación que presenta más baja masa de las tres candidatas, no se encuentran suficientes galaxias satélite en ese mismo rango. Los tres Grupos Locales coinciden en tener una única galaxia en el rango ($M_V < -12$), en el cual las observaciones muestran entre 3-5. En general no obstante, podemos decir que las simulaciones HESTIA resuelven el problema de pérdida de satélites con la inclusión de *feedback* bariónico y la restricción al particular mapa cosmográfico del Grupo Local.

Contents

1 Aim of the work

The ΛCDM model describes galaxies to form in a hierarchical way; small galaxies are the first to form, then subsequently merge into larger and more massive structures (White and Rees, 1978). In this scenario, dwarf galaxies can be seen as survivors of the early universe, and their study is thus crucial to trace, understand and study dark matter, the evolution of galaxies in general, and the ΛCDM universe itself. The Milky Way alone is known to have had several merger events, the most important of them happening 10-12 Gyrs ago, the *Gaia-Enceladus* merger event(Belokurov et al., 2018). However, in the last years discrepancies arise between expectations derived from cosmological simulations and the observed galaxies, which have been baptised as the *small scale crisis* of the ΛCDM model (small meaning $M_{star}<10^9 M_\odot$): (1)simulated galaxies have too many satellites galaxies, in other words, it looks likes we were missing satellites somewhere in our observations. In the past few years, however detection of more and more Ultra Faint Dwarf galaxies (UFDs) and improvement of codes have drastically reduced that discrepancy. This problem is the *missing satellite problem* (Klypin et al., 2009), and right now is alleviated by assuming that the detection limits of the ongoing surveys is still higher than the brightness of UDGs. (2) Further tension arises when studying the internal structure of dwarfs, which have shallower dark matter profiles than predicted from DM only simulations (*Cusp-core problem*).(3) When observing the satellite systems in the MW and Andromeda, satellites appear to rotate having all similar orbit and thus orbiting in a plane rather than randomly. Such planes are simply not expected in cosmological simulations and in a ΛCDM universe, and thus arise a problem called the *planes of satellites problem* (Ibata et al., 2013). Different solutions have been proposed to address this issue: (Libeskind et al., 2015) propose that the planes of satellites align with the large-scale structure and (McCall, 2014) pointed out that the LG is dynamically connected to its environment to the quasi-linear regime of 3-5 Mpc, Shaya and Tully (2013) found that there is a relation between the direction of satellites and evacuation of the Local Void. Other studies point towards a relationship between group infall and planes (Li and Helmi, 2008). More recently, (Sawala et al., 2022) have shown using Gaia proper motions that the orbital pole alignment is actually much more common than previously thought, and reveal that planar structures are transient rather than rotationally supported. What is emphasized here is that accounting for a proper environment for the LG is crucial to set the proper context of study in which we are in. Is the MW a proto-typical spiral galaxy living in $10^{12} M_\odot$ halo? Can the properties we observe in the satellite galaxies surrounding us be extrapolated to other Groups of galaxies, or is our own LG special? How does the major merger event in our galaxy relate to it's characteristics, and what imprint does it leave?

Well, by setting the most correct local environment possible, we first investigate HESTIA (Libeskind et al., 2020) simulation runs to select the initial conditions which best represent the large scale structure of the universe around the LG. This we achieve by comparing the different runs over the observational restrictions given by mass and morphology, distance between two most massive halos MW and M31, star formation history and rates, dark matter, surface brightness and circular velocity profiles. By studying the metal distribution, one gets clear hints about the merger history of certain galaxy, since it leaves its imprint on the metallicity of stars. By matching particular metal distributions to the observed and expected ones, we wish to select the best Local Group candidate in the full suite of simulations.

Secondarily, we are going to investigate the satellites distribution in the suite. These satellites have been born in the context of the Local Group and a controlled cosmographic environment, and are thus a more reliable source of study for the above mentioned problems and more. We aim to investigate weather the satellites form planes, their type of orbits, their times of infall onto their hosts and weather they come in groups ore alone. We also want to count how many satellites there are in the full luminosity range, and if it matches the observations.

2 Cosmological simulations

2.1 Initial conditions

The generation of initial conditions is the first step in cosmological simulation runs. The basic scheme to initialize such simulations could be summarized as follows:

- Choosing a cosmological model (ΛCDM) and setting the cosmological power spectrum of density perturbations $P(k)$.
- Choosing a box size.
- Choosing a number of particles N^3 and putting them down to a regular $N \times N \times N$ grid.
- Choosing a starting redshift z and using the Zeldovich approximation to displace particles according to $P(k)$.

Following the cosmological principle, one should then create an infinite, homogeneous and isotropic universe and superimpose cosmological density perturbations. These density perturbations are usually described by the density contrast:

$$\delta(\vec{x}, t) = \frac{\rho(\vec{x}, t) - \overline{\rho}(t)}{\overline{\rho}(t)} \tag{1}$$

where $\delta(x)$ is ususally decomposed into waves as:

$$\delta(\vec{x}) = \sum \hat{\delta}(\vec{k}) e^{-i\vec{k}\cdot x} \tag{2}$$

$$P(k) = \left\langle \left|\hat{\delta}(\vec{k})\right|^2 \right\rangle_{|\vec{k}|=k} \tag{3}$$

and where $\left|\hat{\delta}(\vec{k})\right|$ is the Fourier transform of the the density contrast. The superposition of long and short waves establishes then the density perturbations of the initial conditions (ICs), as we show in figure 1. This will be of particular importance in our work, since HESTIA simulations are labelled after the seed of the selected long and short waves for the initial configuration of the density field.

Figure 1: Superposition of two waves, one long in green, and one short in purple. The right image shows the result of the sum of both. (Knollmann and Knebe, 2009).

2.2 The HESTIA suite of simulations

Many of the physical processes that drive galaxy formation are already well established in astrophysics. Our actual cosmological model, the Lambda Cold Dark Matter model or simply ΛCDM model, is well established by early universe observations such as the Cosmic Microwave Background, and provides very precise initial conditions. However, from this moment on, starting just after the Big Bang the process of structure formation in the universe is highly non-linear, and in the case of galaxies, governed by the baryons (gas and stars) that live inside the dark matter halos. Different kinds of feedback are thought to be dominant at different mass regimes, so galaxies living in 10^{10} $M_\odot$ halos will be governed by stellar feedback and galaxies living in halos more massive than 10^{12} $M_\odot$ will

be driven by AGN (Active Galactic Nuclei) feedback. In addition to these two kinds of feedback, others such as cosmic rays, radiation pressure can also play a role.

But the process is not only driven by internal processes. Redder early type galaxies, for instance, are thought to live in denser regions than bluer spirals. Galaxies formed in voids are known to be more metal-poor than the average (Pustilnik et al., 2011) and the specific star formation rates is correlated in neighbouring galaxies (Weinmann et al., 2006). So it is apparent that if one wishes to successfully model, say, the Local Group, taking the environment into account should be highly advisable to set up the correct context for that particular galaxies to form.

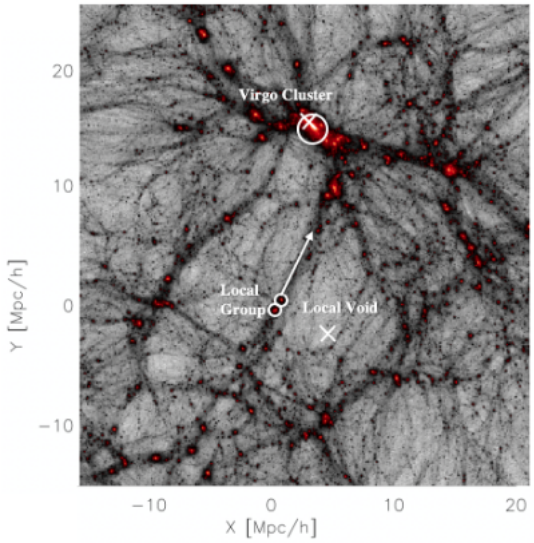

Figure 2: The typical density field in a constrained simulation (Libeskind et al., 2020). The position of the Local void is marked with a white cross as well as the Virgo Cluster. The positions of the main halos of the LG are marked with white circles, and the local filament is determined with an arrow.

The HESTIA simulations (Libeskind et al., 2020), or High-resolutions Environmental Simulations of The Immediate Area, are a set of cosmological simulations of the Local Group, which take into account the particular environment for the formation of MW, Andromeda and its satellites. Such environmental features are selected from a first set of about 1000 DM-only low resolution runs, which are forced to

- include a Virgo Cluster of mass $<2\times10^{14}M_{\odot}$ in a radius within 7.5 kpc.
- A LG-like pair of galaxies of halo mass $8\times10^{11}M_{\odot} < M < 3\times10^{12}M_{\odot}$ no further apart than 500 kpc $< d <$ 1200 kpc, in isolation (no other massive halo within 2000 kpc) and of a halo mass ratio bigger than 0.5.
- To ensure the dominance of the Virgo cluster, no other cluster more massive than Virgo is allowed in a radius of 20 Mpc.

Including this constraint in the simulation, leads to a consistent reproduction of a local filament and a local void, consistent with actual observations, as shown in 2.

HESTIA simulations use the Auriga galaxy formation model (Grand et al., 2016) which use the AREPO code (Springel, 2009). The AREPO code is an accurate and efficient quasi-Lagrangian code which to follow the magnetohydrodynamics of coupled gas and dark matter, the code uses a dynamic unstructured mesh constructed from a Voronoi mesh that allows for a finite-volume discretization of the Euler equations. The MHD equations are solved with second order Runge-Kutta method, and the gravitational forces are calculated with a particle-mesh method in the long range, and with the hierarchical octree algorithm in the short range.

The Auriga galaxy formation model has the following features:

1. Primordial metal-line cooling with self-shielding corrections.
2. The Interstellar Medium, ISM, is modelled as cold dense clouds embedded in a hot ambient medium. When a gas cell exceeds 0.13 particles per cubic cm, it enters in the star formation regime.
3. Star formation follows a Chabrier IMF and occurs stochastically according to a KS-law.
4. The chemical evolution and mass loss is followed through the AGB stars and type I and II supernovae that are distributed in cells around a star particle. The followed elements are H, He, C, N, o, Ne, Mg, Si, and Fe.
5. To include stellar feedback, isotropic winds are launched stochastically from SN type II sites at velocity that scales with the local dark matter velocity dispersion. The energy deposited by this wind is split equally in both kinetic and thermal energy.
6. Black hole feedback is also included. This is achieved by including BHs with masses of $10^5 M_\odot$ in halos of mass greater than $10^{10} M_\odot$ and letting them grow via mergers and nearby gas accretion. The rate of the accretion can be both both quasar or radio mode driven, the former governed by Bondi-Hoyle-Littleton accretion, and the latter by the energy losses of the X-ray halo.
7. A homogeneous magnetic field of 10^{-14} G is seeded in the first instant of the simulation, including a divergence cleaning scheme to ensure $\Delta \cdot B \approx 0$

The simulations use best fit from the Planck collaboration (Ade et al., 2013):

$$H_0{=}100 \cdot h \text{ km/s} \; ; \; h = 0.667$$
$$\sigma_s = 0.83$$
$$\Omega_\Lambda = 0.682$$
$$\Omega_M = 0.318 \text{ for DM-only}$$
$$\Omega_M = 0.270 \; ; \; \Omega_b = 0.048 \text{ for hydrodynamics}$$

After the initial low resolution DM-only runs have established the ICs, these ICs are regenerated with higher resolution, with 4096^3 and 8092^3 effective particles for the medium and high resolution runs, respectively. Each simulation is named with two numbers at the front referring to the seed of the long waves, and two numbers at the back referring to the seed of the short waves. There are in total 24 medium resolution and 3 high resolution runs:

Simulations	Mass resolution [$M_\odot$]	Spatial resolution [pc]
Medium: 01_12, 08_10, 09_10, 09_16, 09_17, 09_18, 09_19 16_10, 16_15,17_10,17_11, 17_13, 17_14, 20_16, 34_13 17_16, 34_14, 37_11, 37_12, 37_16, 37_17, 46_18, 55_02	$M_{dm} = 1.2 \times 10^6$ $M_{star} = 1.8 \times 10^5$	$\epsilon = 340$
High: 09_18, 17_11, 37_11	$M_{dm} = 1.5 \times 10^5$ $M_{star} = 2.2 \times 10^4$	$\epsilon = 220$

Because not all of the medium resolution runs form a LG matching the required conditions, some of them were ruled out, as we will see in section 3.3. Simulations 16_10, 16_15, 20_16, 34_13, 34_14, 46_18, 55_02 are ruled out directly because they fail to reproduce the above mentioned requirements for making a successful LG.

3 Methods

This section explains the methods used to analyze the set of simulations examined in this work in chronological order.

3.1 Halo finder

Group finding is a crucial part in the post-processing of simulations that aim to study structure formation. This work uses *Amiga's Halo Finder* (Knollmann and Knebe, 2009) to identify halos. This is achieved by using an Adaptive Mesh Refinement method in which the density is calculated inside each of the grids defined by an isodensity contour. Once this is done, and after several levels of refinement, one can obtain important halo information such as the virial radius, the halo, gas and stellar masses, the number of particles of each type, the parent halo, and many other physically relevant attributes.

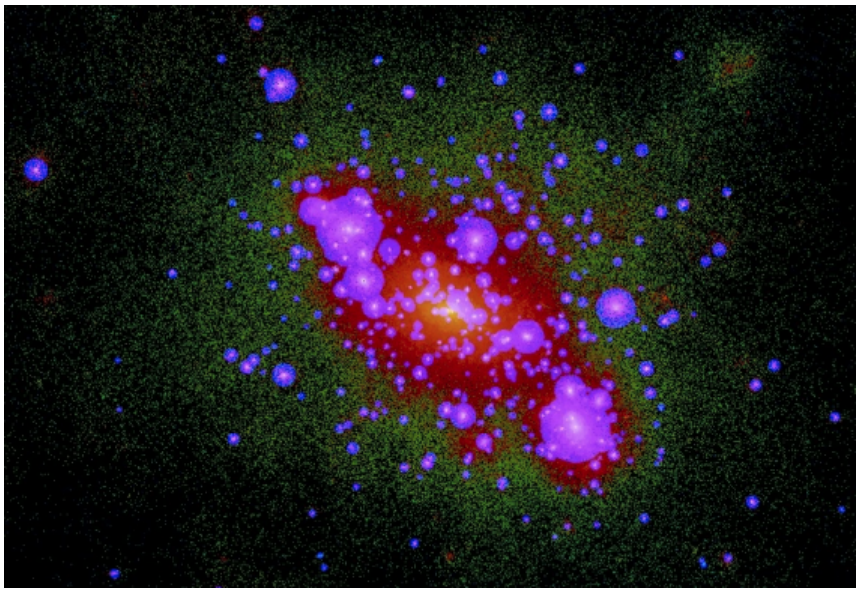

Figure 3: Group finding in a simulated galaxy group with AHF. The host halo is not shown for clarity, and the image is obtained after applying several levels of refinement. The image is taken directly from the AHF documentation (Knollmann and Knebe, 2009).

3.2 Pynbody

Pynbody (Pontzen et al., 2013) is a python module that offers an analysis framework for N-body and hydrodynamic astrophysical simulations, and is used in this work for such purposes.

HESTIA data is stored in different snapshots. Each snapshot corresponds to a different redshift and contains all the relevant information regarding the different particle types or families (stars, gas and dark matter) in that particular evolutionary state of the simulation. Although it is perfectly possible to analyze the snapshots from raw, Pynbody makes the process considerably easier. As HESTIA simulations are powered by the AREPO code, rather than PKDGRAV/Gasoline, Gadget, Gadget4/Arepo or N-Chilada, data storage has slight peculiarities with respect with the mentioned codes and some small modifications had to be made in Pynbody's settings in order for it to correctly function.

Once this was done, we first center the simulation in one of the main halos (MW or M31) and work from there. Primarily used properties are positions and velocities, mass fractions of different chemical abundances (namely oxygen, hydrogen and iron) and age or redshift. Additionally, pynbody offers a very powerful image function, with which one can easily create renders of the different families. A very interesting function for our study, is the possibility of aligning a particular galaxy both edge and face on, because it allows us to study the presence (or absence) of a disk structure.

It is important to note that the first part of this work is restricted to the last snapshot stored, corresponding to $z = 0$, and for the second part, we loop over the rest of snapshots available to trace particles across them.

3.3 Searching for LG candidates

As mentioned above, some criteria in order to select successful LGs had to be established. We look for couples of halos that are massive, meaning $M_{vir} = 7 \times 10^{11}$-$2 \times 10^{12}$ of high resolution `fmhighres` ≥ 0.98 and in a distance range of around $d = 600 - 1000$ kpc.

ID	M_{M31}	M_{MW}	M_{MW}/M_{M31}	$M_{star,M31}$	$M_{star,MW}$	d
	$[10^{12}M_\odot]$	$[10^{12}M_\odot]$		$[10^{10}M_\odot]$	$[10^{10}M_\odot]$	[kpc]
01_12	2.93	2.53	0.863	12.7	12.1	721
08_10	2.06	1.25	0.607	9.85	5.53	856
09_16	2.07	1.25	0.603	9.28	6.40	756
09_17	2.27	1.31	0.577	9.79	7.03	1088
09_18	2.22	1.92	0.865	1.02	8.52	884
09_19	2.15	1.22	0.567	9.25	5.25	724
17_10	2.16	2.08	0.963	9.24	1.13	736
17_11	1.56	1.33	0.852	8.85	7.99	656
17_13	2.08	1.89	0.907	9.80	8.67	978
17_14	1.49	1.40	0.939	8.93	6.19	613
37_11	1.12	1.11	0.991	5.05	6.24	860
37_12	1.22	0.99	0.811	6.66	5.04	843
37_16	1.11	1.08	0.973	5.20	5.10	727
37_17	1.23	0.97	0.788	5.81	5.00	810
09_18	2.13	1.94	0.911	13.2	11.2	866
17_11	2.30	1.96	0.852	13.1	11.8	675
37_11	1.04	1.02	0.981	5.61	5.99	850

Table 1: The most relevant values for every LG that made the first cut. The distance is calculated from centre to centre, using the centre of mass as reference.

Observational data restricts the mass of the Milky Way usually to 1.0-2.1 $[10^{12}M_\odot]$ (Hattori et al., 2018), but this is still a very much discussed topic among astrophysicist. More precise measurements have been made, (Battaglia et al., 2005) , for instance, restrict the mass to $0.8^{+1.2}_{-0.2}$ $[10^{12}M_\odot]$, or in (Kafle et al., 2014) to $0.80^{+0.31}_{-0.16}10^{12}\times M_\odot$. Andromeda, on the other side, is estimated to be in the 0.6-2.0 range (Corbelli et al., 2010) and values of mass ratios of smaller to bigger halo therefore in the 0.5-1.0 range. Note that the M_{star} values are somewhat larger than in the HESTIA paper (Libeskind et al., 2020) due to they using only stars in the galactic disk. The total stellar mass estimate is M_{star} =6.08± 1.14×$10^{10}M_\odot$ (Licquia and Newman, 2014). With this in mind, one can already see how the first candidates start to gradually fall away: 01_12, for example, looks already way to massive, both in virial mass and in stellar mass. All the other galaxies seem to overcome this first mass filter.

Putting the information in the table 1together, we are able to represent all pairs of galaxies in the typical M_{star} vs M_{halo} plane, also known as abundance matching 4, along with the relationship obtained by (Kravtsov et al., 2018), calculated through scattered abundance matching (meaning the most massive galaxy is not supposed to live directly in the most massive halo, but rather in a range of mass centered in its mass) as well as the observational constraints. The technique of abundance matching, as its name already says, matches observed distributions of stellar masses to the total mass distributions of simulated halos assuming halos having higher stellar mass, also live in the most massive halos.

We find our pairs of galaxies to fit in reasonably well in this Kravtsov's (Kravtsov et al., 2018) abundance matching relation. All of them exhibit stellar masses in the upper range of the scatter, but the agreement is very satisfactory. Note how high resolution galaxies also have higher masses at $z = 0$ and are in the limit of the observational ranges, at least 09_18 and 17_11. The gap in the M_{halo}≈1.4-1.9 $M_\odot$ range is not for physical reasons,

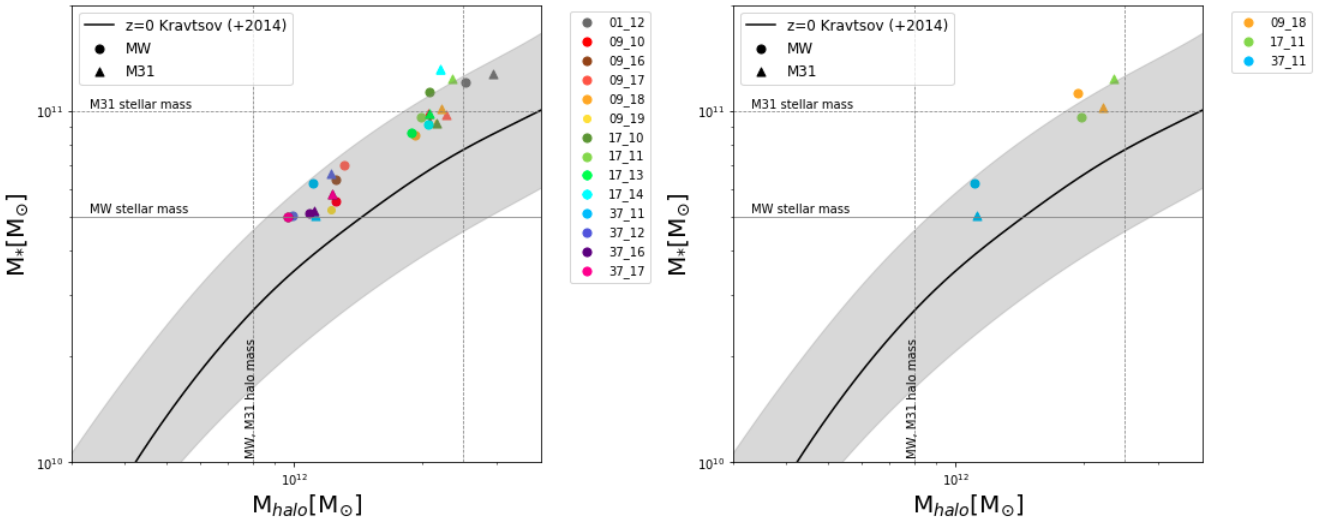

Figure 4: The M_{star} vs M_{halo} relation for the medium (4096^3) and high (8192^3) resolution HESTIA LGs. The black solid line is the M_{star} vs M_{halo} relation in (Kravtsov et al., 2018), and the gray are the uncertainty at 1σ.

but just an effect for the small number of realizations of the distributions, according to the authors (Libeskind et al., 2020).

The distance is observationally quite well constrained to 785 ± 25 kpc according to McConnachie (2012b), range in which more ore less most of the local groups fit in. By adopting a very relaxed criteria for the distance selecting all pairs of galaxies within d$= 600 - 1000$ kpc, we only rule out 09_17 in the distance filter.

We also check that our galaxies have NFW dark matter profiles 5. The full profiles will be shown in the next section, but this is just added as an anticipation.

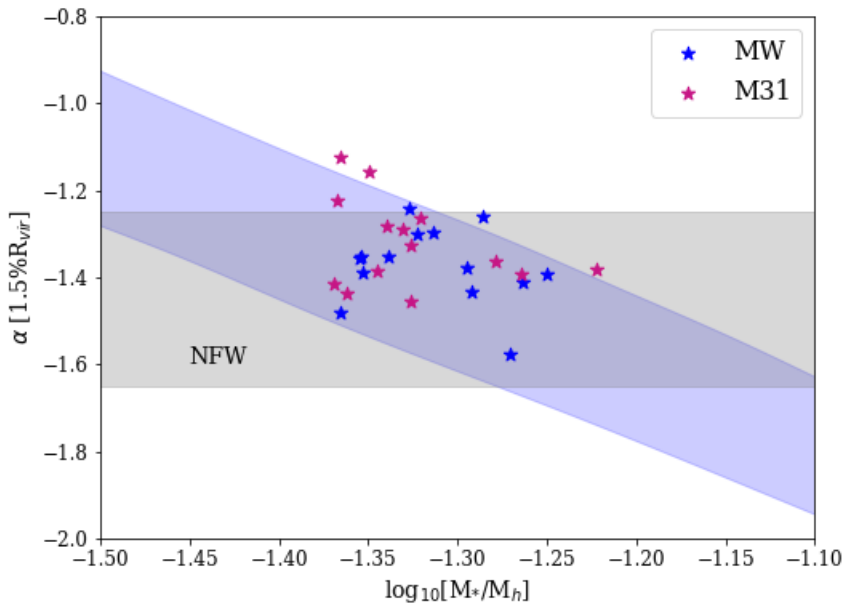

Figure 5: Plotted is the inner dark matter density slope α at r $= 0.015$ R_{vir} as a function of M_{star}/M_{halo} for the simulated galaxies at $z = 0$. The gray area shows the expected slope of dark matter NFW profiles, while the shaded blue area is the 1σ scatter obtained from NIHAO simulations in (Tollet et al., 2015).

3.4 Metal abundances

Stars make up to just 4% of the Milky Way's mass (the rest is mainly dark matter, and some gas and dust) but are essential to study the different evolutionary stages of it. The history of our host galaxy is written in them, and will only reveal to the careful reader.

The local stellar halo (defined as a sphere within 2 kpc from the Sun) is long known to be composed of two distinct stellar populations. This was first noted using the Hiparcos data (Chiba and Beers, 2000) and later on confirmed via Hertzprung-Russel diagrams. First of all, one must have a large spectroscopic data catalogue and be able to resolve individual stars. Using H3 Survey spectroscopy and Gaia astrometry (Gaia DR2) and fitting into the CMD, reveald more hints about events occurred in the Milky Way. The diagram shows two distinct main sequences: one shifted more to the red, with respect to the other, shifted to the bluer part. The red population is usually also referred to as the *in-situ* population because it was formed in the main progenitor (*proto*-Milky Way) whereas the blue population are thought to be stars accreted in the major merger event underwent 10-12 Gyrs ago(Brook et al., 2020) (Gallart et al., 2019). The kinematical distinction here, is that *in-situ* stars have much less eccentric and prograde orbits, whilst accreted stars have much higher eccentricity in their orbits and are retrograde (going against the bulk rotation trend of the Milky Way) (Conroy et al., 2022).

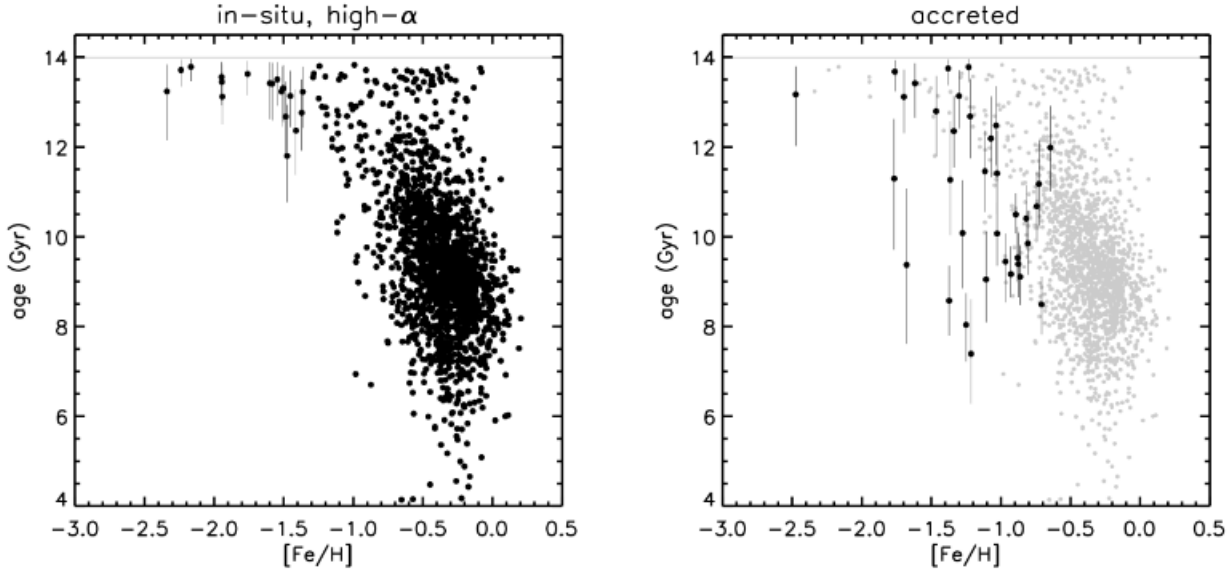

Figure 6: Age of the i*n-situ*, high-α(left panel) and accreted (right panel) stars as a function of metallicity.from the H3 survey(Conroy et al., 2022). The authors use kinematic arguments to distinguish between both components. In-situ stars are defined to have prograde orbits (L_Z <0) with eccentricities e¡0.8, while accreted stars are defined to have e >0.9 or a combination of e >0.8 and L_Z >500 km/s/kpc (retrograde orbits). The *in-situ* population is uniformely very old until [Fe/H]< −1.3, and then spans in a wide range of ages. The accreted component, in contrast, shows stars younger that 12 or even 10 Gyrs aven at metallicities lower than [Fe/H]< −1.3 .

But it's not kinematics but we will focus in here, but rather chemical abundances. As we have said, we have to distinct stellar populations in the milky ways disk;

- sequence of red stars that were heated during GSE from in main progenitor and are related with the thick disk (*in-situ*)
- a blue sequence formed by stars belonging to the accreted galaxy (Matteo et al., 2019)

The study of metals is key for this study. It is known that α elements (C, O, Ne, Mg, Si, S) only form in TypeII supernovæ, which happen in dying massive stars exclusively. On the other hand, iron, or simply Fe, will form in both TypeII and TypeI (from WD binaries) supernovæ, meaning any dying star releases Fe into the interstellar

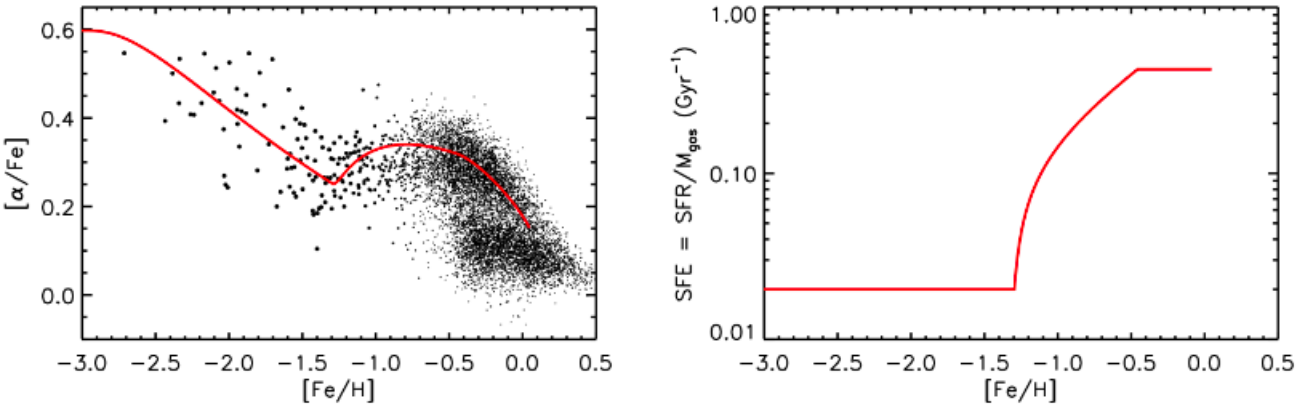

Figure 7: Tinsley-Wallerstein diagram for the stars showed in the previous figure, also from (Conroy et al., 2022). The model is shown in red to stress the hump happening then the iron content in the MW was of around [Fe/H]≈1.3. The right panel shows how the model translates the alpha element increase translates into a boost in SFR.

.

medium. There is therefore a difference in the timescale of release to the ISM: Iron is released steadily in the long timescale, and α elements, on the other hand, in rapid timescale due to the fact that massive stars are short-lived. This implies two things:

First of all, that there is a correlation between stellar age and [Fe/H] content in stars, meaning older stars have lower metallicities, and it increases as dying stars release more and more Fe into the ISM (6, left panel)

Second , that in the beginning of the universe, alpha elements must dominate over iron, but as time passes by, iron content must slowly catch up and eventually at some point dilute the alpha element content. In fact, this can be seen in the Tinsley-Wallerstein diagram, or just [α/H] vs [Fe/H] plane. One would expect on the one hand stars with low Fe and high α to gradually become stars with high Fe and low α.

This is exactly what happens, at least to one point: When the metallicity in our home galaxy was of about [Fe/H]$\approx$ 1.3 something peculiar seems to happen. The [α/Fe] vs [Fe/H] plane suddenly exhibits a hump, a sudden enhancement in α elements that can be understood as a sudden burst in star formation 7. A lot of fresh , big hot stars emerge and also die rapidly, liberating their α to the ISM and promptly increasing the [α/Fe] ratio.

The next question in an easy one. Why? Well, there is still debate here, but one of the most promising option is the fact that a major merger initiated this sudden peak of star formation rates. As many previous studies have shown, for instance (Di Cintio et al., 2021), infalling satellites onto main host galaxies and merger events are indeed able to trigger episodes of intense star formation.

3.4.1 Selecting the local neighborhood

In order to study the metal distribution of the local stellar halo, one must first determine the position of the sun. In simulations tho, there is not a specific star particle determined as the Sun, and therefore a certain volume has to be defined in which potential suns are placed in the simulation. Knowing that the Sun's galactocentric distance is of $d = 7.98 \pm 0.15$ kpc (Malkin, 2012), we define a volume with

$$r_{GC} = [7, 9]\, kpc \quad z = [-1, +1]\, kpc \tag{4}$$

to ensure we select sun-like stars only. This volume is sometimes also referred to as solar annulus.

3.4.2 Transformation of metal abundance data

Another issue to cope with in the transformation of chemical abundances, since the snapshots in HESTIA contain information about the mass fraction of every element present, and this kind of studies are usually conducted using logarithmic quantities. The transformation we use is the following:

$$\left[\frac{A}{B}\right] = \log\left(\frac{X_A}{X_B}\right) - \log\left(\frac{X_A}{X_B}\right)\Big|_\odot \tag{5}$$

where we have used the solar abundances from (Nicolas and Anders, 1989):

$$\frac{X_{Fe}}{X_H}\Big|_\odot = \frac{0.00125}{0.706} \quad \frac{X_O}{X_{Fe}}\Big|_\odot = \frac{84}{12.4} \tag{6}$$

3.5 Milky Way satellites

The Milky way has over 40 confirmed satellite galaxies, but it is thought there could be many more with the discovery of more and more ultra faint galaxies. These companion galaxies code much information about the Milky Way itself, in the sense that they can for example give restrictions for its mass (Fritz et al., 2020) using their proper motions.

Recent studies show how these proper motions could be actually much lager than previously thought ((Kallivayalil et al., 2018), (Hammer et al., 2021)) which could lead to the fact that most Milky Way satellites are *newer* than expected, or in other words, it is unusual for satellites to be long term companions of the Milky Way before infalling. In this work, we are interested to study weather there is any correlation between satellite velocity and infall time, or satellite mass and infall time, see when the satellites are captured by the host halos, and if they come alone or in groups.

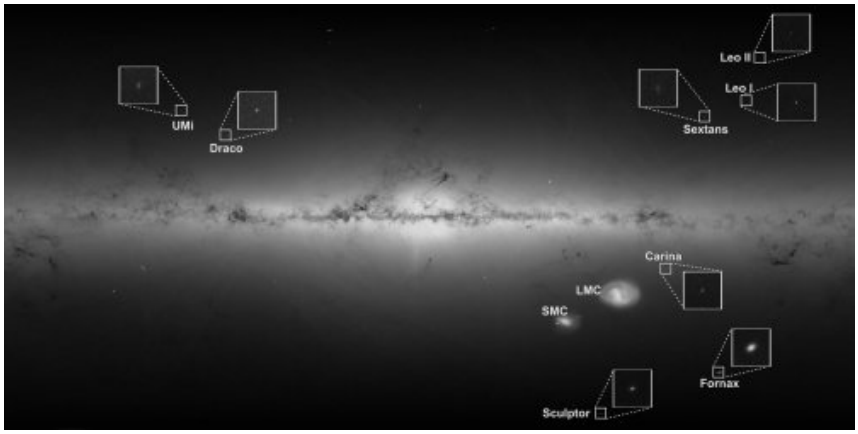

Figure 8: Image of the Milky way and its satellites from Gaia EDR3. Classical dwarf spheroidals are labelled as well as the LMC and SMC. ESA/Gaia/DPAC, CC BY-SA 3.0 IGO

3.5.1 Selecting and tracing Milky Way satellites

To try and study the kinematics and longevity of the satellites in HESTIA suite of simulations, we first need to identify them. In this work, we select all halos inside the virial radius R_{vir} at $z = 0$, which of course will change from simulation to simulation. The halo finder sometimes mistakes gas blobs with actual halos, and so a second

requirement is that the baryonic to dark matter ratio is:

$$r = \frac{M_{gas} + M_{star}}{M_{dm}} < 0.1 \tag{7}$$

to ensure there is sufficient dark matter. A third an last requirement for the selected galaxies is to have at least $M_{star} > 10^6 \mathrm{M}_\odot$ in order to be sure that there is enough resolution and stellar particles in each studied satellite. Once this is done, we calculate their rotation velocities with:

$$v_{rot} = \frac{v_x\, y - v_y\, x}{\sqrt{x^2 + y^2}} \tag{8}$$

Because selecting the full set of star particles in a given halo would lead to including stars that are not bound enough and thus get stripped away, we select 10 star particles in the very center of each satellite and calculate their mean rotational velocity. Two types of motion are then distinguished: prograde orbits defined to have positive values of v_{rot} and retrograde orbits, which have negative v_{rot}. The positive values of v_{rot} are defined as prograde because they rotate in the same direction as the galactic disk.

To trace the satellites throughout the different snapshots in time, we select an old star pertaining to it, and another star in the centre of the MW. Because each individual particle has an individual identification number in the simulation stored in the `iord` array, that won't change from snapshot to snapshot, it is possible to detect the two selected stars at any point in the simulation. By doing so, we determine the distance between all pairs of stars at every z and compare it to the virial radius, to determine the moment each satellite enters the virial radius for the first time.

4 Results

This section exposes the obtained results in chronological order. Because the number of analyzed simulations in rather large, and for the sake of the continuity in the text, we prefer to show only 3 of the simulations in this section (the 3 high resolution ones) and show the rest of them in the appendix A.

4.1 The best Milky Way candidate

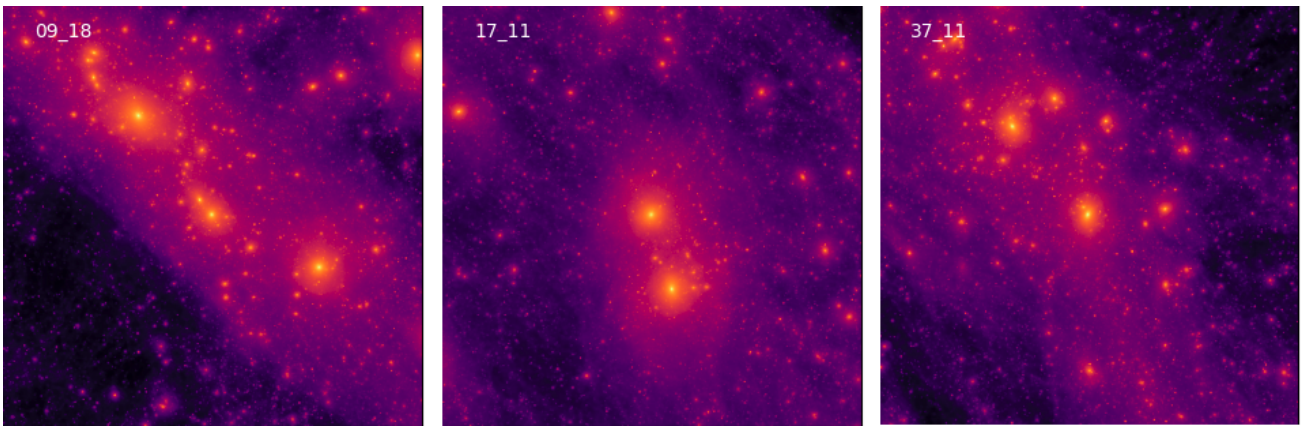

Figure 9: Dark matter density in $M_\odot/\mathrm{kpc}^{-2}$ for the three high resolution HESTIA LGs (19_18, 17_11 and 37_11) at $z = 0$. Panels are 3 Mpc across and centered on the MW. The two main galaxies are seen in the center, formed in a dark matter filament.

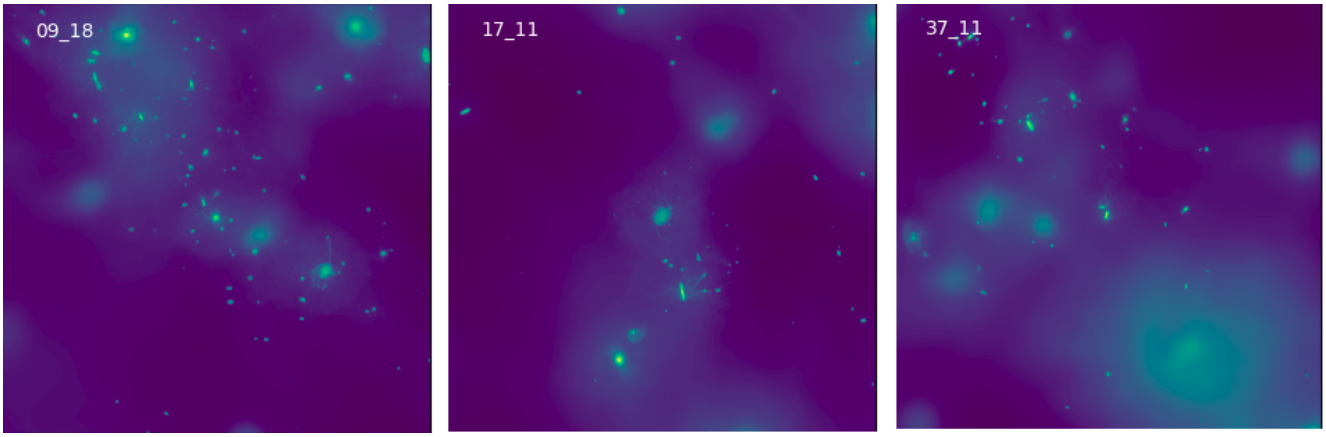

Figure 10: Gas density for the three high resolution HESTIA LGs (19_18, 17_11 and 37_11) at $z = 0$. Panels are 3 Mpc and centered on the MW. The two main galaxies are seen in the center, surrounded by smaller orbiting satellites

.

For having a first glance at each individual Local Group, we plot the gas and dark matter across the 3 Mpc 9, which shows the dark matter filament where each group lives in. The full gas distribution tells us what galaxies are gas rich and which not10. Once we have this, we obtain the plot for each individual main host MW/M31, face and edge on 11, 12. We already observe how some of the LGs show irregular gas distributions such as 01_12, 09_16, 09_17, 09_19, 37_16 or 37_17, or big blobs around at $z = 0$, which we link with possible mergers at this time, and makes us to rule them out. Others do not exhibit thin disks like 09_17, 09_19 at $z = 0$ which is also not a good sign for the local groups to be satisfactory.

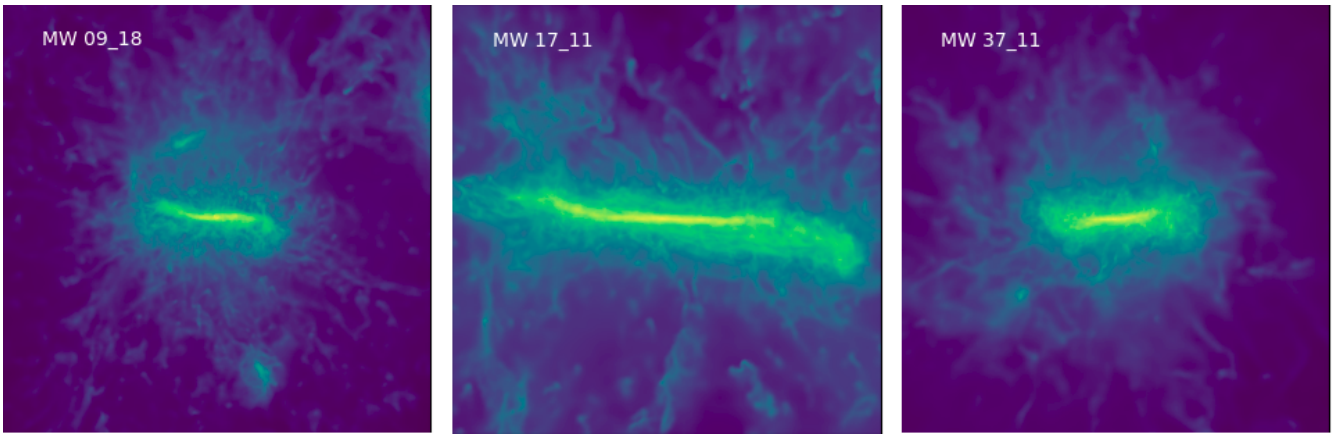

Figure 11: Edge on images of the selected MW candidates. Higher gas density in yellow shows the gas aligning in a thin disk, surrounded by some lower density green colored gas. Scale of the box is 75 kpc across

.

With this criteria, a calm rotating gas distributed in a thin disk at $z = 0$, most promising candidates should be 09_10, 09_18, 17_10, 17_11, 17_13 and 37_11. Note that these selected medium resolution LGs, also include the only three selected LGs run at higher resolution 24,25, 26, 27, 28.

The mass accretion history provides a second restriction to the local group selection. The Milky Way's mass accretion history is yet unknown and very difficult to determine observationally, but there is an important constraint to it: the *Gaia-Enceladus* merger event that happened at around 10-12 *Gyrs* ago. Thus, we seek for galaxies which will exhibit important mass accretion at that time, corresponding to roughly $z = 1.5 - 3$. From the full suite, we see how most of them have accreted at least 90% of their mass at already 5 Gyrs ago. For our 6 selected hosts in the morphology cut, we have a look at the mass accretion history for their Milky Ways, and rule out 09_18 which

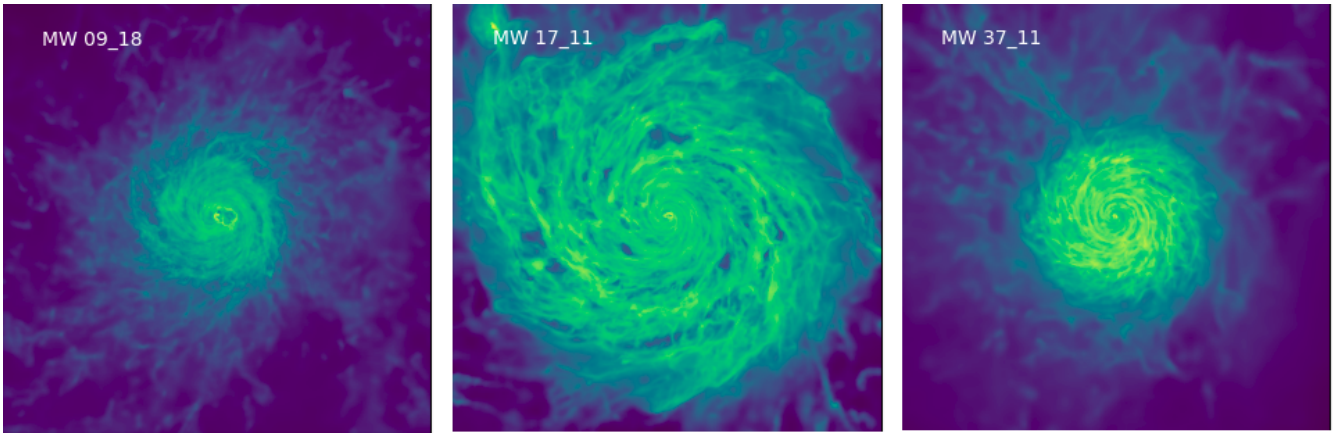

Figure 12: Edge on images of the selected MW candidates. Higher gas density in yellow shows the gas aligning in a thin disk, surrounded by some lower density green colored gas. Scale of the box is 75 kpc across

.

exhibits strong mass accretion at $z = 0$ 13.

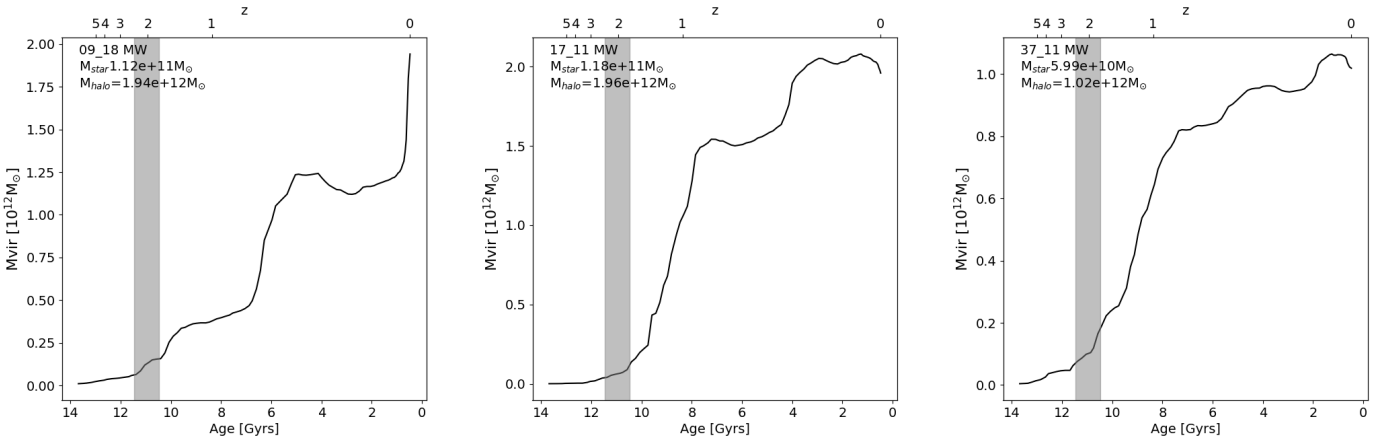

Figure 13: Mass accretion history of the selected MW candidates. Lookback time in the X axis includes a mark at 10 Gyrs denoting estimated GSE merger time. Labels show star and total mass of the galaxy at $z = 0$.

.

For the dark matter density and surface brightness profiles 1415 we just investigated two things: (1) the dark matter profile is fit well by a NFW profile

$$\rho(r) = \frac{\rho_0}{\frac{r}{R_S}(1 + \frac{r}{R_S})^2} \tag{9}$$

(2) the surface brightness profile fits well to a Sèrsic profile

$$I(r) = I_e \cdot \exp\Big[- b_n \Big[\big(\frac{r}{R_e}\big)^{1/n} - 1 \Big] \Big] \tag{10}$$

to the approximate bulge, which we fit to the inner 10 kpc. We obtain for the remaining candidates expected values for late type spiral galaxies 1415. The Sèrsic index n controls the curvature of the $I(r)$ profile, smaller n values giving shallower curves. The values for the inner slope α_{NFW} of NFW profiles of all candidates is plotted in 5, and is obtained performing a linear fit to the inner 1%-2% of R_{vir}.

The mass accretion history is a necessary but not sufficient condition to establish the right context for the MW's

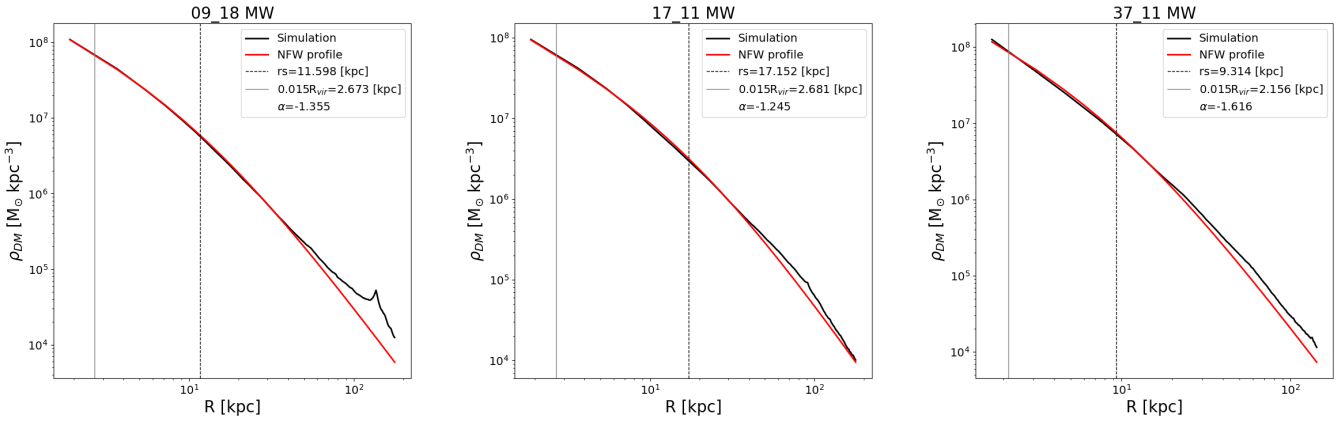

Figure 14: The dark matter profiles of the simulated MW candidates are modelled by a NFW profile, in red, from $0.015R_{vir}$ (gray line)to the R_{vir}. The label shows the best fitting values of the scale radius (dotted line) aswell as the inner slope α, which has been computed from 1% to 2% of the virial radius.

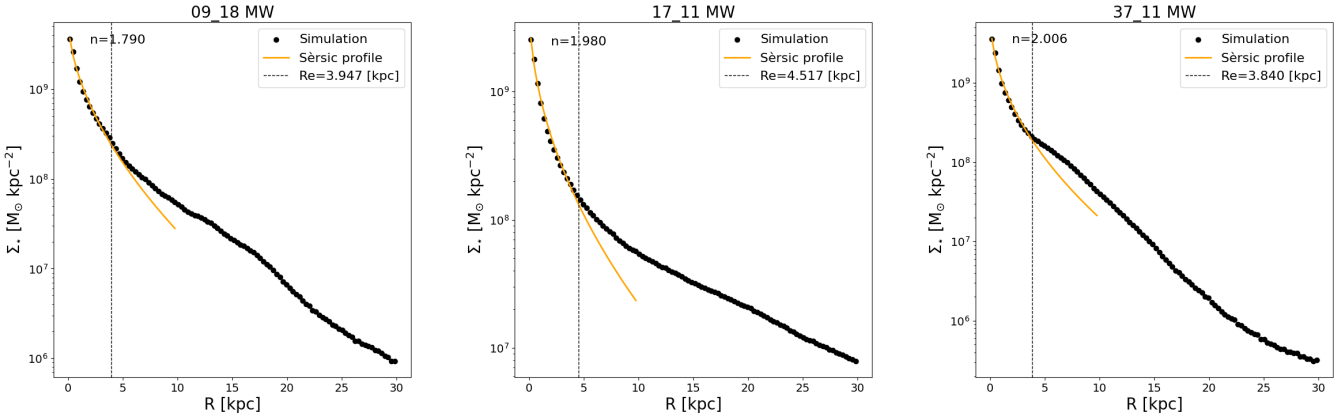

Figure 15: The surface brightness profile is modelled by a single Sèrsic profile usually used to describe bulges. The bulge effective radius is computed in the label, and marked with a vertical dotted line. The values of the Sèrsic index n are also added in the plot.

.

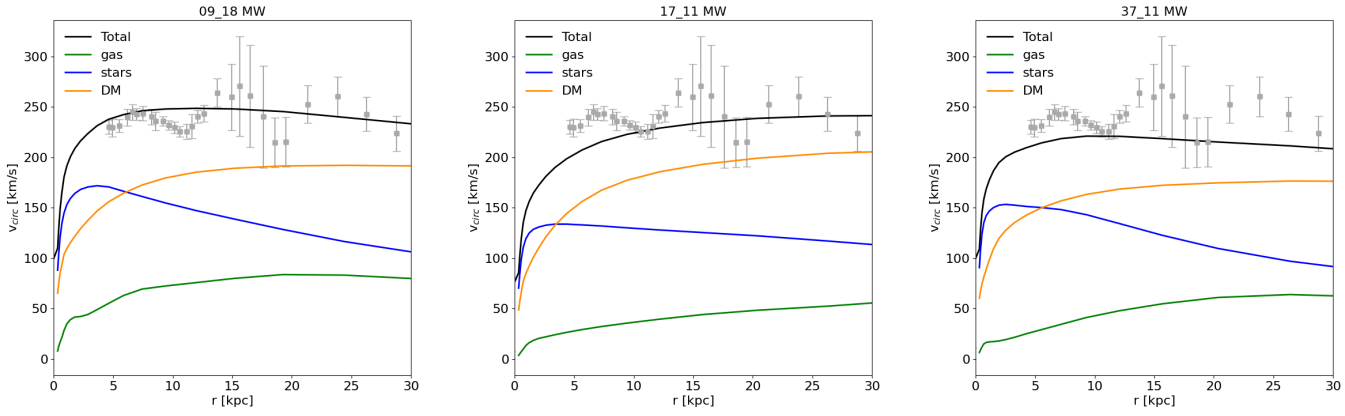

Figure 16: Circular velocity of the three high resolution MW analogues. The total circular velocity is drawn as a black line, while the gas, star and dark matter are drawn in green, blue and orange, respectively. Observational data is from (Liu et al., 2016).

past accretion history. Snaith et al. (2014) point out that the MW's star formation history had an important burst at around 10 Gyrs ago, and has remained low and practically constant for the rest of its evolution. With this in mind we try to select candidates that fit in in this description.

As we have already pointed out, large mergers contribute to heating of the galactic disk and bursts of star formation, which must be reflected in the metallicity of the disk. First of all, it is important to note that all of the $[Fe/H]$ vs age planes 17 show a clear main sequence, this is, stars that have formed inside the main progenitor. There is an important broadness in all cases, consistent with the quasi-Lagrangian scheme they implement which is characterized by weaker metal mixing than Eulerian ones. If there is at some point in the evolution of the galaxy in which there is an accreted component, one should observe a clump of lower metal content followed by a starburst, this is, a higher density of stars born at that time. Because the main sequences are so broad, we are not able to distinguish between accreted and *in-situ* populations and we have to rely solely on the higher density regions to identify possible mergers. Also, as previous works have pointed out, Sarrato (2022), this can be due to the fact that accreted galaxies in HESTIA of lower mass than the MW candidates show an excess of stars that increase the metallicity of its stars through nuclear reactions and sends them to the same spot on the $[Fe/H]$ vs age plane. The $[O/Fe]$ vs $[Fe/H]$ plane is closely related to the age metallicity plane. As we have already commented, bursts of star formation will as well bring a lot of big massive stars to the galaxy, which will soon die and and liberate α elements to the environment, so that after every merger one should observe the so-called *elbow* (sometimes also referred to as *knee*), a sudden change in the general negative slope of the plane.

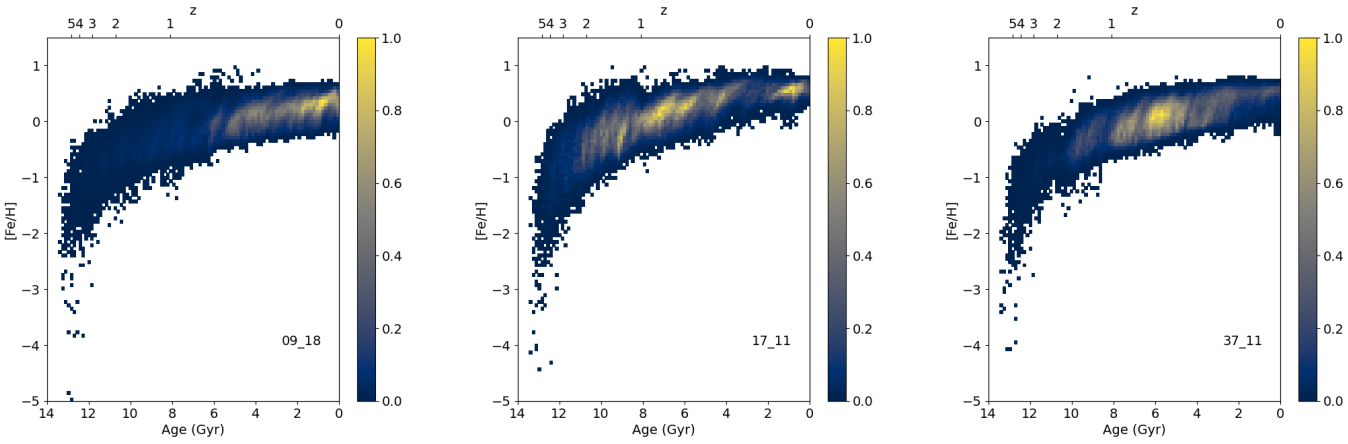

Figure 17: [Fe/H] versus age for the selected solar neighborhood stars of the three high resolution MW candidates. Solar neighborhood is taken to be stars in donut-shape between $[7, 9]$ kpc and z height $[-2, -2]$ kpc. The histogram is normalized, and a colorbar is included in the right-hand side, where 0 represents bins with 1 star and 1 the maximum number of stars found in a bin. 37_11 shows a clump of lower metallicity stars at 10-8 Gyrs which could be a merger. Same happens for 09_18 but at 8-6 Gyrs.

.

Looking at our five remaining candidates, we note that 09_10 has had mainly recent star formation ($t_{lookback} < 4$ Gyrs). This is also reflected in its alpha element production, which does not show the typical and desired *elbow*. So, we are left with 17_10, 17_11 and 17_13, 37_11. From comparison of their age-metallicity plane for the low mass halo, we observe how 37_11 is probably the one with the neatest star formation history, forming most of its stars from 10 Gyrs to roughly 4 Gyrs ago 19 . This is also backed up in the $[O/Fe]$ plane, in which we see a *hump* at $[Fe/H] \approx -1$. Other candidates, 17_10, 17_11, 17_13 have much messier star formation histories and do not show such behavior.

Another factor playing in favor of 37_11 rather than 17_11 is its dimensions. From figure 12 we observe how 17_11 would be almost the full 75 kpc across, but recent works like (Schuller et al., 2020) size it in around 40 kpc across and 2 kpc thick, (Kafle et al., 2014) say the stellar halo shows a break at R=$17.2^{+1.1}_{-1.0}$ kpc, (Amôres et al.,

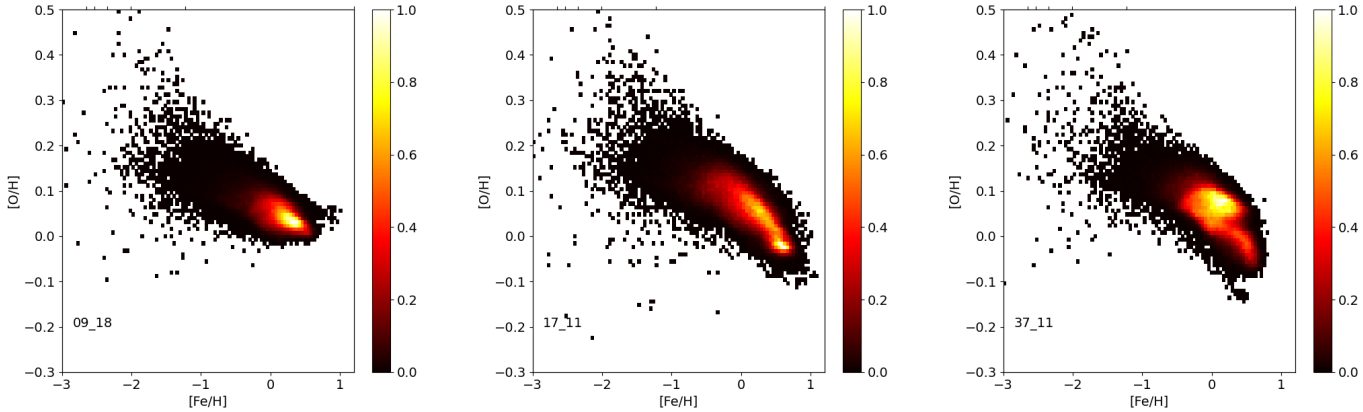

Figure 18: [O/Fe] versus [Fe/H] for the selected solar neighborhood stars of the three high resolution MW candidates. Solar neighborhood is taken to be stars in a donut-shape between $[7, 9]$ kpc and z height $[-2, -2]$ kpc. The histogram is normalized, and a colorbar is included in the right-hand side, where 0 represents bins with 1 star and 1 the maximum number of stars found in a bin. Again, we observe hints of mergers in 37_11, since there is significant boost in alpha elements around [Fe/H]≈-1

.

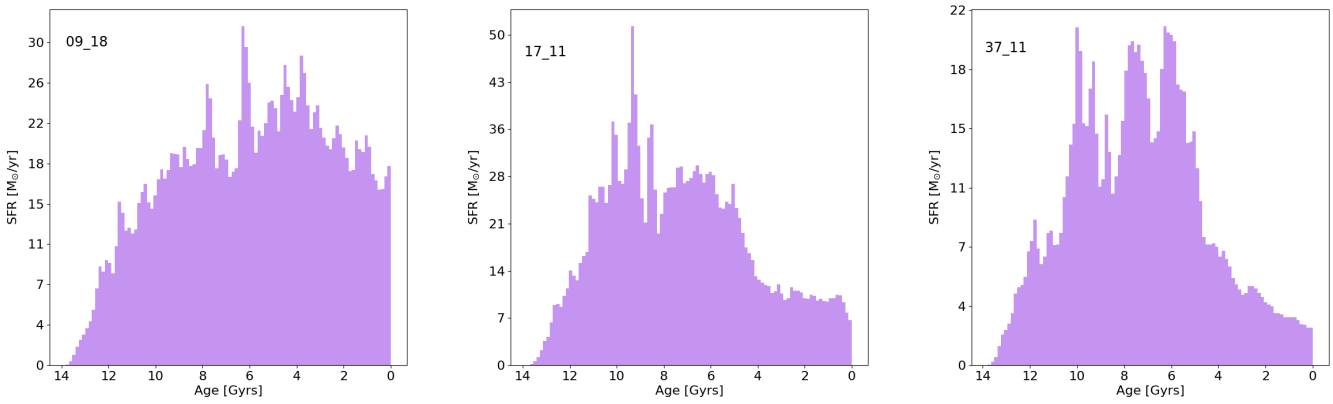

Figure 19: Star formation history for the three high resolution galaxies 09_18, 17_11 and 37_11. As predicted in the Tinsley-Wallerstein diagrams 18 09_18 has mostly recent star formation activity, and 37_11 forms most if its stars between 10 and 4 Gyrs. 17_11 shows very high SFR at 10 Gyrs. Each histogram is composed of 100 bins.

.

2017) size it in $R = 16.1 \pm 1.3$ kpc based on the Two Micron All Sky Survey, or (Minniti et al., 2011) in $R = 13.9 \pm 0.5$ kpc considering the clump giants of the disc as standard candles, calibrated from Hipparcos parallaxes. As 17_11 occupies the full panel which is 75 kpc across, it would have a R of about 35 kpc, which doubles the observed radius.

A final proof we subject our local groups to is matching the observed circular velocity data. As one can see from figure 16, most of the galaxies have total circular velocities in the range constrained by observations, as has our favourite candidate 37_11. The observational data from the panels is from (Liu et al., 2016). The paper also includes best fit for the virial mass of the Milky Way from a mass model they construct based on the rotation curve shown in 16. They estimate the virial mass in $M_{vir} = 0.90^{+0.07}_{-0.08} 10^{12} \times M_{\odot}$, similar to the one study conducted by (Kafle et al., 2014) which is $M_{vir} = 0.80^{+0.31}_{-0.16} 10^{12} \times M_{\odot}$ and in excellent agreement with 37_11. The stellar mass in given in (Licquia and Newman, 2014) is also in very good agreement with the of 37_11.

4.2 Milky Way satellite systems

In this section we address the following questions regarding the satellite systems (with $M_{star} > 10^6 M_\odot$) in MW/M31:

a) How are the satellites distributed space-wise in the *face-on* (XY) and *edge-on* (XZ) planes of their hosts? Is there any particular or preferred direction, or planar structure?

b) Do satellites in such systems show any particular tendency towards having prograde/retrograde orbits?

c) Is there any correlation between the orbit type (prograde/retrograde) and the mass in stars M_{star}? Is there any correlation between the orbit type and the time of first infall (t_{infall}) in the virial radius of the hosts? Is there any other correlation with the infall time of the satellites, such as with the module of v_{rot} at $z = 0$?

d) Is there any correlation between group infall and planes of satellites?

e) Are HESTIA simulations able to correctly simulate the observed Luminosity Function of the Milky Way and Andromeda? Are such constrained simulations able to give a solution to the long lasting *missing-satellite* problem?

4.2.1 Planes of satellites

All the satellites we show in this section are subjected to the restrictions from the previous section 3. First of all, we want to analyze the position of each of the satellites in the XY plane to see if there is some kind of alignment in them, or favourite orientation with respect to the plane of the disk of each host galaxy (we define the XY plane to be the plane containing the disk of the galaxy). From figure 21 we see that the most massive local groups ($M_{17\_11} > M_{09\_18} > M_{37\_11}$) also have the richest satellite systems as seen in the below table.

LG	host	$n_{satellites}$ ($n_{prograde s}$)	M_{vir} [$10^{12} M_\odot$]	M_{MW+M31}[$10^{12} M_\odot$]
09_18	MW	8 (4)	1.94	4.07
	M31	8 (5)	2.13	
17_11	MW	9 (4)	1.96	4.26
	M31	12 (5)	2.30	
37_11	MW	6 (3)	1.02	2.07
	M31	1 (1)	1.04	

From just visual inspection, it looks like there could be some kind of alignment in the M31 analogues in 09_18 and 17_11 21 . The XZ plane shows how in both cases a preferred alignment around the z axis, but when one looks at the velocities, the arrows do not seem to point in same direction, neither do satellites have same module of v_{rot} orbits. This disparity in the kinematics makes us think that it could be more of transient effect due to the low number statistic. Nevertheless, it is not to left unseen that in 17_11 M31 and 09_18 M31 both show alignment in the z axis and 09_18 MW in the x axis. To quantify this alignment, we take the satellites inside the range $x_i \in$[-20, 20] kpc in the reference system of figure 21 and count the number of satellites inside that range. (Ibata et al., 2013) say that the Andromeda galaxy shows 50% of its satellites aligned in a thin disk of scatter < 14.9 kpc, so we also include the satellites included in a more narrow range of $x_i \in$[-10, 10] kpc. We see the results in the following table.

Host	$n_{x\in[-20,20]kpc}$	$n_{x\in[-10,10]kpc}$	$n_{z\in[-20,20]kpc}$	$n_{z\in[-10,10]kpc}$
09_18 MW	5/8	4/8	-	-
09_18 M31	-	-	7/8	4/8
17_11 M31	-	-	8/12	5/12

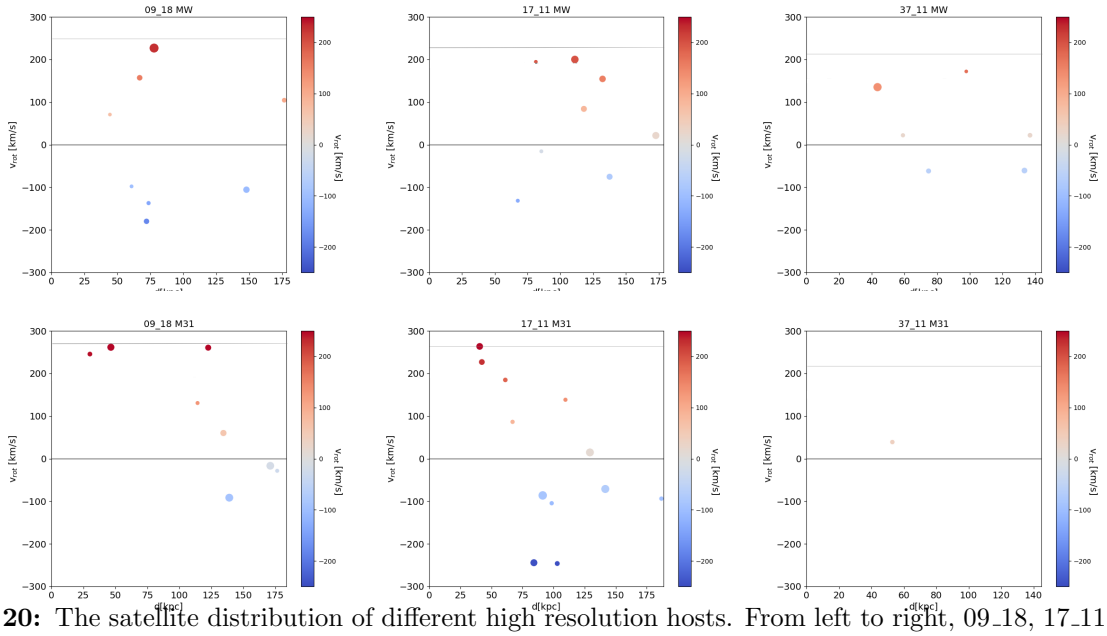

Figure 20: The satellite distribution of different high resolution hosts. From left to right, 09_18, 17_11, 37_11 and from top to bottom, the Milky Ways (which is just the low mass halo in the pair) and Andromeda (M31). All selected satellites are inside the virial radius of its host galaxy, and have M_{star} values grater than 10^6 $M_\odot$. There is a continuum line at 0 [km/s] and a gray line at the total circular velocity of each galaxy.

which could, or could not hide planar structures of satellites. No particular alignment is observed for the rest of candidates. This, of course, should be a issue of deeper and more rigorous study, since (1) the number of hosts studied is very low, and (2) there are outliers to the alignment and they are just studied from visual inspection (3) planar structured galaxies show very unalike kinematics. On another note, it looks like the satellites do not show preferences to have pro or retrograde orbits since the numbers seem to be particularly evened out.

Regarding the radial distance of each satellite form their host's center, there is a very balanced 20/46 ratio (43%) of satellites orbiting at a distance $d <$R$_{vir}/2$, so it does not look like they prefer to orbit at certain distances from their hosts.

We do not find satellites with M_{star} more massive than 10^9M$_\odot$. Only 1 satellite is as massive as 10^8M$_\odot$ in stellar mass, and the rest is in the 10^6M$_\odot$-10^8M$_\odot$ range, being 22/46 $M_{star} < 10^7$M$_\odot$ and and 23/46 10^7M$_\odot$ $<M_{star} < 10^8$M$_\odot$.

Apart from more massive halos having richer satellite systems, the satellites also appear to have larger modules for v_{rot}. 20.

4.2.2 Tracing and infall times

Once the satellites are well identified and their properties known, it is time to look at them in the past. As we have stated already, we are interested at the times the satellites cross the virial radius for the first time, the infall time, which we will call t_{infall}. Panels 22 show the relative distance at which each of the satellites is at every snapshot in the simulation, that is, its orbit. The computation time is very high in this cases since every computation implies looping over a number of halos of the order of 10^5 and calculating their positions, to later select only those which match the criteria and use all the different snapshots at different z to determine their position relative to the main host. For this reason, we only perform the study of satellites for the six high resolution hosts.

There is disparity of phenomena going on in figure 22. First of all, we examine how most satellites have their first infall t_{infall} at roughly 2-6 Gyrs, this is, more than 8 Gyrs ago. There is only 3 satellites that have been

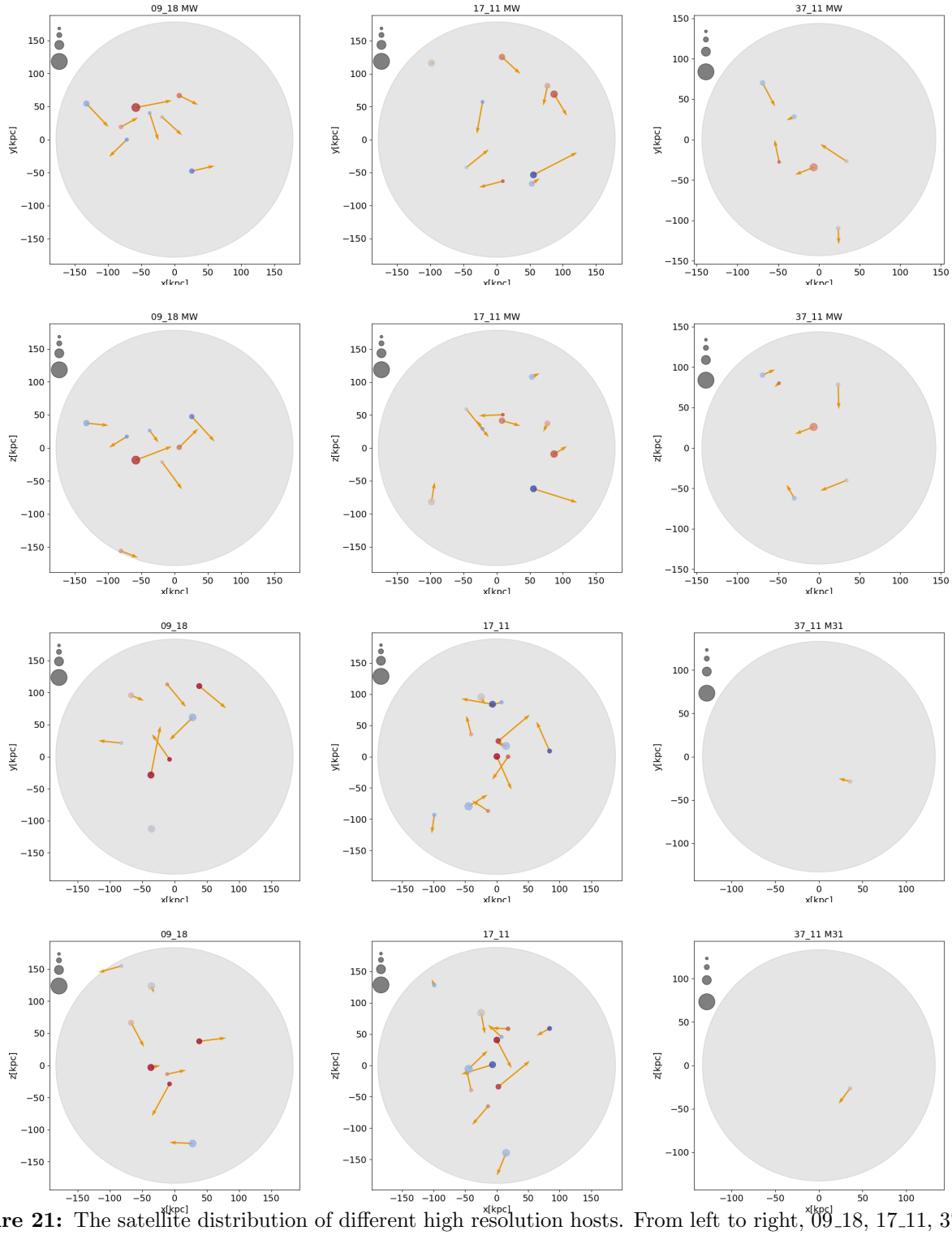

Figure 21: The satellite distribution of different high resolution hosts. From left to right, 09_18, 17_11, 37_11 and from top to bottom, the Milky Ways (which is just the low mass halo in the pair) and Andromeda (M31). All selected satellites are inside the virial radius of its host galaxy, and have M_{star} values grater than 10^6 $M_\odot$. Red satellites have prograde orbits with positive rotation velocities, blue satellites have negative rotation velocities and retrograde orbits. The colorbar is the same as for figure 20. The gray symbols in the top left corner are for visual comparison with, from top to bottom, what a galaxy with 10^6,10^7,10^8,10^9 would look like. The orange vectors give us an idea of the satellites direction of movement at $z = 0$ and are computed with the two components of velocity corresponding to each of the axes of the shown XY and XZ planes.

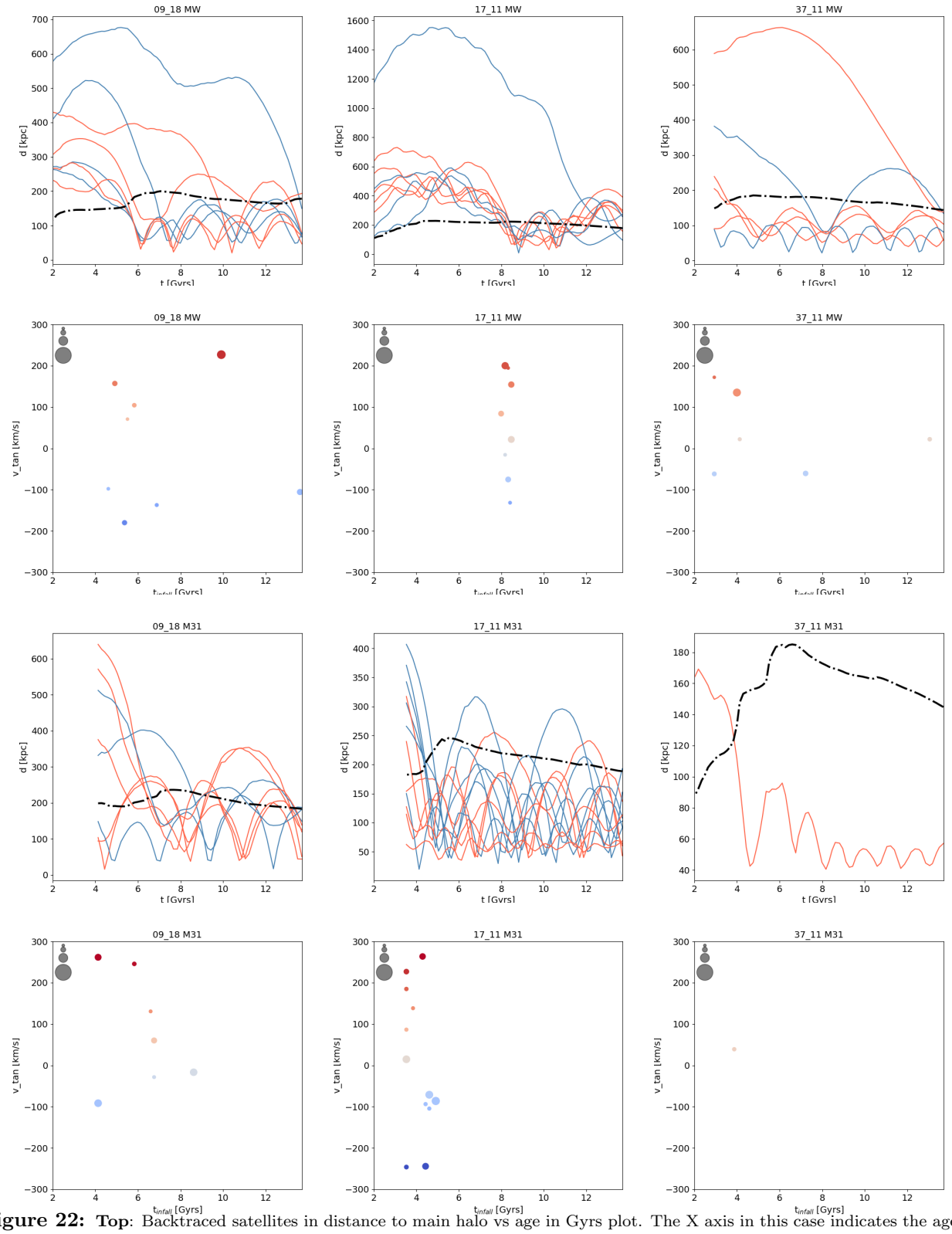

Figure 22: **Top**: Backtraced satellites in distance to main halo vs age in Gyrs plot. The X axis in this case indicates the age of the universe. The satellites that are prograde at $z = 0$ are maintained red for their full orbits, and so are the blue. The black dash-dotted line is the virial radius at every point, in kpc. Like before, top row corresponds to satellites in the MW with star mass bigger than 10^6 solar masses, and the bottom row are the satellites in Andromeda.

accreted in the past 2 Gyrs.

In the range of t_{infall} we obtain for all satellites, we first ask weather there is correlation between M_{star} and the infall time, as one would expect and previous works have shown (Wetzel et al., 2015). This correlation is expected in the ΛCDM universe, since more massive halos are more common at later cosmic times, and thus are also expected to fall in later into the host halo, which is also growing as time passes. Also, satellites that are more massive have also shorter dynamical-friction timescales and are thus expected to merge earlier with their hosts. No such correlation is observed in HESTIA simulations. Both halos of M_{star} =10^6 $M_\odot$ and M_{star} =10^7 $M_\odot$ appear to enter the virial radius of their host at similar times, looking at figure 22, whose symbol sizes are related to the Mstar of each satellites. We caution the reader that we are looking at a rather small range of stellar masses, therefore it can be expected that a strong correlation is not seen.

Second, we examine whether satellites that have higher module of v_{rot} at $z = 0$ are also more likely to be accreted before. From the panels shown in 23, there looks like there is no particular correlation between these two quantities.

There is, nevertheless, a large number of backsplashed satellites, backsplash meaning satellites that entered the virial radius of the host at some point to then later exceed it again at least once. We find that 14/46 ≈1/3 of the total satellites are backsplashed, from which 8 have prograde orbits at $z = 0$ and 6 retrograde. No particular preference for backsplashed satellites to be prograde or retrograde is thus apparent from these numbers.

Finally, a striking event happens in three of the hosts: there is a clear group infall in both the MW candidates of 09_18 and 17_11 and the M31 analogue in 17_11. Group infall appears to happen at a range of different epochs in general, since for instance in 17_11 M31 it happens at around 4 Gyrs, in 09_18 at 6 Gyrs and in 17_11 MW at 8 Gyrs. The M31 analogue in 09_18 also shows a smaller group of 3 satellites falling in at approximately 7 Gyrs. Such group infall has lately been postulated to account for the peculiar disk-like distribution of satellites observed in the local group (Klimentowski et al., 2010) and is also often also linked to accretion via mergers. A surprisingly high number of satellites is accreted in group, namely 20/46, which represents roughly 44%. Also, one can see from the figure 22 that satellites seem to group *before* or just shortly after they first fall into the virial radius of their respective host. The just mentioned local groups are the ones (not 09_18 MW) which also have the most aligned satellite systems, so group infall could indeed trigger the formation of planes of satellites, as studied in some works mentioned earlier. A further investigation of this possibility is highly desirable in a future work.

4.2.3 Luminosity function

We now proceed to compute the total luminosity function of satellites within MW and M31, by considering all galaxies - even the ultra faint ones- and integrating the total magnitude of each halo, we obtain the result in figure 23. This result is obtained maintaining the ratio of baryonic to dark matter lower than 0.1. Overplotted are the observational Luminosity Functions from (Bennet et al., 2019). We see how in the $M_V < -14$ there is a generalized lack with respect to observations. The simulations reproduce 1 satellite each in this regime, while in observations we find between 3-5. In the $M_V > -14$ range on the other side, we see how the simulated hosts in HESTIA are able to reproduce well the observations. 17_11 is the best fitting option, having over 20 satellite galaxies for both MW and M31 with M_V <-7. Following closely we see 09_18, which also has over 10 galaxies in the same range of magnitude for the MW, and around 15 for the M31. 37_11 shows fewer satellites than expected observationally. Eliminating the mass filter to select hosts in all mass ranges only increases the number of satellites from 1 to 4 in M31 in comparison to the section presented before, and from 6 to 10 for the MW.

Overall, the result is very promising, in the sense that it shows the ability of HESTIA simulations, by being run over a controlled cosmographic landscape (Virgo Cluster, Local Void, Local Filament), to create the correct environment for the main hosts MW and M31, and thus to correctly account for the number of satellites in the Local Group hosts. This naturally solves the missing satellite problem, which typically occurs only in N-body, dark

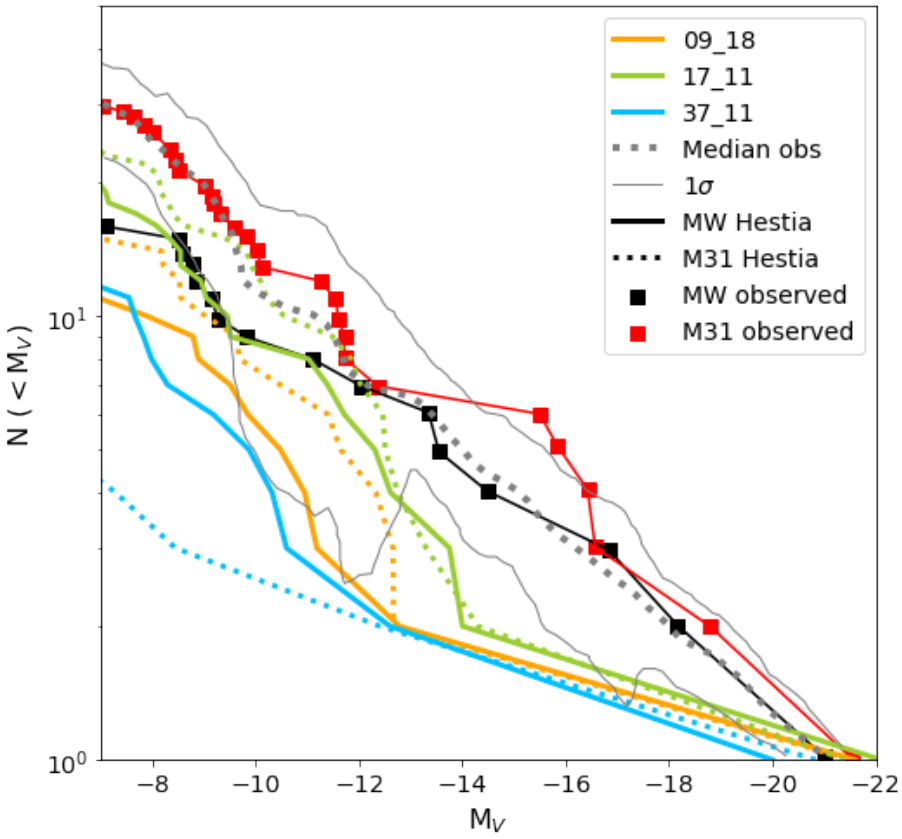

Figure 23: The cumulative luminosity function for the Milky Way (solid) and M31 (dotted) analogues in the Hestia high resolution simulations. Overplotted is the observed luminosity function as presented in (Bennet et al., 2019) for MW in black, and M31 in red. The dotted gray line is the median obtained in the article, and thin gray lines indicates the 1σ scatter of that median. The data for the MW is taken from (McConnachie, 2012a) and for M31 from (Martin et al., 2015). All the satellites included are the ones found inside the virial radius R_{vir} and down to $M_V \approx -7$

.

matter only simulations.

5 Summary & discussion

Using the HESTIA environmental hydrodynamic suite of simulations, we examine the high (3 local groups) and medium resolution (24 simulations, of which only 15 reproduce the Local Group satisfactorily) Milky Way and Andromeda analogues. We rule out 10 of the medium resolution runs because they do not match the observed characteristics, and restrict our study to the rest of candidates. We summarize our primary results as follows:

1. We find the best fitting Milky Way to be the one in simulation 37_11, based on its virial mass, stellar mass, velocity curve, morphology, dark matter density profile, surface brightness profile, star formation history, mass accretion history and metal distribution. The main characteristics of the mentioned LG can be resumed in the following table:

Host	M_{M31}	M_{MW}	M_{MW}/M_{M31}	$M_{star,M31}$	$M_{star,MW}$	d	$\alpha_{NFW,MW}$	n_{Sersic}	v_{diskMW}
	$[10^{12}M_\odot]$	$[10^{12}M_\odot]$		$[10^{10}M_\odot]$	$[10^{10}M_\odot]$	[kpc]			[km/s]
37_11	1.04	1.02	0.981	5.61	5.99	850	-1.616	2.01	212

   The values of α_{NFW} shown are values for the inner slope of the DM density profile computed from a linear fit from 1% to 2% the virial radius. The value n_{Sersic} is the Sèrsic index of the bulge fitted to the inner 10 kpc. The value for the total circular velocity of the galaxies is computed from the flat part of the circular velocity profile. In both cases, these values are within the expected range for late-type spiral galaxies. The selected galaxy is in excellent agreement with virial mass estimates obtained from rotation curve measurements from (Liu et al., 2016) and (Kafle et al., 2014). It is also in very good agreement with stellar mass estimate from (Licquia and Newman, 2014). Also, it shows evidence for a major merger event that occurred around 8 Gyrs ago, later than GSE is thought to happen. As we will see in the following section and have already seen in the results section, the local group does not match the observed distribution of satellites in the Luminosity Function. Additionally, it is desirable to check whether the drastic decrease in number of satellites is correlated to the mass of the hosts in any way or not.

   The more massive and bigger candidate 17_11 on the other hand, reproduces the luminosity function much better. It also shows a very strong peak in SFR around 10 Gyrs and keeps stiller for the rest of its life, in better agreement with (Snaith et al., 2014), and also agrees with more recent observational virial mass estimates from Watkins et al. (2019) $M_{vir} = 1.54^{+0.75}_{-0.44}10^{12}M_\odot$. It is not in agreement with radius estimates from (Kafle et al., 2014), (Amôres et al., 2017), (Minniti et al., 2011).

2. We study the $z = 0$ distribution of the satellite systems in our main MW/M31 hosts. The more massive hosts also have the richest satellites systems; 16 in 09_18, 21 in 17_11 and 7 in 37_11 with $M>10^6M_{star}$ and baryonic to dark matter fraction < 0.1. The results obtained can be summarized as follows:

   a) Three hosts show a particular alignment in their satellite system, namely MW 09_18 and and M31 09_18 and 17_11. The thickness of the observed planes and the kinematical disparity of the satellites forming them implies that these structures might be rather transient than supported by rotation, as (Sawala et al., 2022) says.

   b) Of the total of 46 satellites found, 22 have prograde orbits ($v_{rot} >0$) and 24 have retrograde orbits ($v_{rot} <0$) at $z = 0$, so no particular tendency appears to underlay.

   c) No correlation between the orbit type and the mass, rotational velocity at $z = 0$ nor time of first infall onto the virial radius is inferred. Most of the satellites have their first infall in the first 2-6 Gyrs of

evolution, meaning they fall into the virial radius at roughly z>1. Only 3/46 satellites fall into the virial radius in the last 2 Gyrs. Given the small range of mass analyzed, we did not expect a strong correlation anyways.

d) There happens to be 4 out of the 6 high resolution hosts with a group infall of some of the galaxies infalling into them. The times of these group infalls are largely varying; for 09_18 it happens at 6 Gyrs for the MW and 7 Gyrs for M31 (note in this case time is not given in lookback time, but in age of the universe) and for 17_11 MW at 8 Gyrs and M31 at 4 Gyrs. Group preprocessing and infall appears to be a very common event in such satellite systems since 43% of all the satellites are accreted in this way. 3 out of 4 hosts with group preprocessing do also show possible planar structures. Both M31 candidates in 09_18 and 17_11 show roughly 87% and 66% of their satellite galaxies confined to a $x \in [-20, 20]$ kpc plane respectively, and MW in 09_18 has 62% of its satellites in $z \in [-20, 20]$ kpc. The numbers drop drastically when narrowing the planes to $z \in [-10, 10]$ kpc and $x \in [-10, 10]$ kpc, to 50% in both the MW and M31 analogues and 42% in 17_11 M31. The low number of realizations and the inhomogeneity in kinematical characteristics of such satellites induces us to leave this issue to adress in a more careful and rigorous study.

e) The Luminosity Function of the Milky Way and Andromeda is well described by HESTIA, primarily by the two most massive local groups 09_18 and 17_11. No *missing satellites* problem is found here. We would say that there is indeed the opposite effect; there is a *missing simulated satellite* problem in any case, since 37_11 falls short in number of satellites with $M_V < -7$. In summary, we can say that when taking into account the *correct* environment, as well as the implementation of baryonic feedback such as reionization and supernovae for the Local Group to form, the number of satellites appears to naturally also adjust better to the observed distribution.

6 Aknowledgements

I would like to thank Arianna and Chris for their guidance throughout this work, and their time spent on answering my doubts and giving me feedback. Also big thanks to Noam Libeskind who gave us very valuable information to start and work with HESTIA simulations. To my family who has always supported me both financial and morally, to Naroa for listening to me when things were not going that good, and last but not least, thanks to my second family, David, Javi, Alfredo and Amaiur, who helped me out immensely when I decided to start this journey.

References

Peter Ade, N. Aghanim, Charmaine Armitage-Caplan, Morel Arnaud, Mark Ashdown, F. Atrio-Barandela, Jonathan Aumont, Carlo Baccigalupi, A. Banday, Ramon Barreiro, J. Bartlett, E. Battaner, K. Benabed, A. Benoît, Aurélien Benoit-Lévy, J. Bernard, M. Bersanelli, P. Bielewicz, and A. Zonca. Planck 2013 results. xvi. cosmological parameters. *Astronomy Astrophysics*, 571, 03 2013. doi: 10.1051/0004-6361/201321591.

E.B. Amôres, Annie Robin, and C. Reylé. Evolution over time of the milky way's disc shape. *Astronomy & Astrophysics*, 602, 02 2017. doi: 10.1051/0004-6361/201628461.

Giuseppina Battaglia, Amina Helmi, Heather Morrison, Paul Harding, Edward Olszewski, Mario Mateo, Kenneth Freeman, John Norris, and Stephen Shectman. The radial velocity dispersion profile of the galactic halo: Constraining the density profile of the dark halo of the milky way. *Monthly Notices of the Royal Astronomical Society*, 364:433 – 442, 12 2005. doi: 10.1111/j.1365-2966.2005.09367.x.

V. Belokurov, D. Erkal, Neil Evans, Sergey Koposov, and A.J. Deason. Co-formation of the disc and the stellar halo. *Monthly Notices of the Royal Astronomical Society*, 478:611–619, 07 2018. doi: 10.1093/mnras/sty982.

P. Bennet, D. Sand, D. Crnojević, K. Spekkens, A. Karunakaran, Dennis Zaritsky, and Burcin Mutlu-Pakdil. The m101 satellite luminosity function and the halo–halo scatter among local volume hosts. *The Astrophysical Journal*, 885:153, 11 2019. doi: 10.3847/1538-4357/ab46ab.

C. Brook, Daisuke Kawata, Brad Gibson, Carme Gallart, and Andrés Vicente. Explaining the chemical trajectories of accreted and in-situ halo stars of the milky way. *Monthly Notices of the Royal Astronomical Society*, 495: 2645–2651, 07 2020. doi: 10.1093/mnras/staa992.

Masafumi Chiba and T. Beers. Kinematics of metal-poor stars in the galaxy. iii. formation of the stellar halo and thick disk as revealed from a large sample of non-kinematically selected stars. *Astronomical Journal*, 119, 03 2000.

Charlie Conroy, David Weinberg, Rohan Naidu, Tobias Buck, James Johnson, P. Cargile, Ana Bonaca, Nelson Caldwell, Vedant Chandra, Jiwon Han, Benjamin Johnson, Joshua Speagle, Yuan-Sen Ting, Turner Woody, and Dennis Zaritsky. Birth of the galactic disk revealed by the h3 survey, 04 2022.

E. Corbelli, S. Lorenzoni, R. Walterbos, Reinaldo Braun, and Thilker A. A wide-field h i mosaic of messier 31. *http://dx.doi.org/10.1051/0004-6361/200913297*, 511, 02 2010. doi: 10.1051/0004-6361/200913297.

Arianna Di Cintio, Robert Mostoghiu, Alexander Knebe, and Julio Navarro. Pericentric passage-driven star formation in satellite galaxies and their hosts: Clues from local group simulations. *Monthly Notices of the Royal Astronomical Society*, 506, 06 2021. doi: 10.1093/mnras/stab1682.

T Fritz, Arianna Di Cintio, G Battaglia, C. Brook, and Salima Taibi. The mass of our galaxy from satellite proper motions in the gaia era. *Monthly Notices of the Royal Astronomical Society*, 494:5178–5193, 06 2020. doi: 10.1093/mnras/staa1040.

Carme Gallart, Edouard Bernard, C. Brook, Tomás Ruiz-Lara, Santi Cassisi, Vanessa Hill, and Matteo Monelli. Uncovering the birth of the milky way through accurate stellar ages with gaia. *Nature Astronomy*, 3:1, 10 2019. doi: 10.1038/s41550-019-0829-5.

Robert Grand, Facundo Gómez, Federico Marinacci, Ruediger Pakmor, Volker Springel, David Campbell, Carlos Frenk, Adrian Jenkins, and Simon White. The auriga project: the properties and formation mechanisms of disc galaxies across cosmic time. *Monthly Notices of the Royal Astronomical Society*, 10 2016. doi: 10.1093/mnras/stx071.

Francois Hammer, Jianling Wang, Marcel Pawlowski, Yanbin Yang, Piercarlo Bonifacio, Hefan Li, Carine Babusiaux, and Frédéric Arenou. Gaia edr3 proper motions of milky way dwarfs. ii: Velocities, total energy and angular momentum. *The Astrophysical Journal*, 922, 12 2021. doi: 10.3847/1538-4357/ac27a8.

Kohei Hattori, Monica Valluri, Eric Bell, and Ian Roederer. Old, metal-poor extreme velocity stars in the solar neighborhood. *The Astrophysical Journal*, 866:121, 10 2018. doi: 10.3847/1538-4357/aadee5.

Rodrigo Ibata, Geraint Lewis, Anthony Conn, Michael Irwin, Alan McConnachie, Scott Chapman, Michelle Collins, Mark Fardal, Annette Ferguson, Neil Ibata, A Mackey, Nicolas Martin, Julio Navarro, R Rich, David Valls-Gabaud, and Lawrence Widrow. A vast, thin plane of corotating dwarf galaxies orbiting the andromeda galaxy. *Nature*, 493:62–5, 01 2013. doi: 10.1038/nature11717.

Prajwal Kafle, Sanjib Sharma, Geraint Lewis, and Joss Bland-Hawthorn. On the shoulders of giants: Properties of the stellar halo and the milky way mass distribution. *The Astrophysical Journal*, 794, 08 2014. doi: 10.1088/0004-637X/794/1/59.

Nitya Kallivayalil, Laura Sales, Paul Zivick, Tobias Fritz, Andrés Pino, Sangmo Sohn, Gurtina Besla, Roeland Marel, Julio Navarro, and Elena Sacchi. The missing satellites of the magellanic clouds? gaia proper motions of the recently discovered ultra-faint galaxies. *The Astrophysical Journal*, 867:19, 10 2018. doi: 10.3847/1538-4357/aadfee.

Jarosław Klimentowski, Ewa Łokas, Alexander Knebe, Stefan Gottlöber, Luis Martinez-Vaquero, Gustavo Yepes, and Yehuda Hoffman. The grouping, merging and survival of subhaloes in the simulated local group. *Monthly Notices of the Royal Astronomical Society*, 402:1899 – 1910, 03 2010. doi: 10.1111/j.1365-2966.2009.16024.x.

Anatoly Klypin, Andrey Kravtsov, Octavio Valenzuela, and Francisco Prada. Where are the missing galactic satellites? *The Astrophysical Journal*, 522:82, 01 2009. doi: 10.1086/307643.

Steffen Knollmann and Alexander Knebe. Ahf: Amiga's halo finder. *The Astrophysical Journal Supplement Series*, 182, 05 2009. doi: 10.1088/0067-0049/182/2/608.

A. Kravtsov, A. Vikhlinin, and Alexander Meshcheryakov. Stellar mass—halo mass relation and star formation efficiency in high-mass halos. *Astronomy Letters*, 44:8–34, 01 2018. doi: 10.1134/S1063773717120015.

Yang-Shyang Li and Amina Helmi. Infall of substructures on to a milky way-like dark halo. *Monthly Notices of The Royal Astronomical Society - MON NOTIC ROY ASTRON SOC*, 385:1365–1373, 04 2008. doi: 10.1111/j.1365-2966.2008.12854.x.

Noam Libeskind, Yehuda Hoffman, R. Tully, Helene Courtois, Daniel Pomarède, Stefan Gottloeber, and Matthias Steinmetz. Planes of satellite galaxies and the cosmic web. *Monthly Notices of the Royal Astronomical Society*, 452, 03 2015. doi: 10.1093/mnras/stv1302.

Noam Libeskind, Edoardo Carlesi, Robert Grand, Arman Khalatyan, Alexander Knebe, Ruediger Pakmor, Sergey Pilipenko, Marcel Pawlowski, Martin Sparre, Elmo Tempel, Peng Wang, Hélène Courtois, Stefan Gottlöber, Yehuda Hoffman, Ivan Minchev, Christoph Pfrommer, Jenny Sorce, Volker Springel, Matthias Steinmetz, and Gustavo Yepes. The hestia project: simulations of the local group. *Monthly Notices of the Royal Astronomical Society*, 498, 09 2020. doi: 10.1093/mnras/staa2541.

Timothy Licquia and Jeffrey Newman. Improved estimates of the milky way's stellar mass and star formation rate from hierarchical bayesian meta-analysis. *The Astrophysical Journal*, 806, 07 2014. doi: 10.1088/0004-637X/806/1/96.

Xiaowei Liu, Haibo Yuan, Maosheng Xiang, Huawei Zhang, Bingqiu Chen, Juanjuan Ren, Chun Wang, Yong Zhang, Yonghui Hou, Yuefei Wang, and Zihuang Cao. The milky way's rotation curve out to 100 kpc and its constraint on the galactic mass distribution. *MNRAS*, 463, 04 2016. doi: 10.1093/mnras/stw2096.

Zinovy Malkin. The current best estimate of the galactocentric distance of the sun based on comparison of different statistical techniques. 02 2012.

Nicolas Martin, David Nidever, Gurtina Besla, Knut Olsen, Alistair Walker, A. Vivas, Robert Gruendl, Ricardo Muñoz, Robert Blum, Abhijit Saha, Blair Conn, Eric Bell, You-Hua Chu, M. Cioni, Thomas Boer, Carme Gallart, Shoko Jin, Andrea Kunder, Steven Majewski, and Dennis Zaritsky. Hydra ii: a faint and compact milky way dwarf galaxy found in the survey of the magellanic stellar history. *The Astrophysical Journal*, 804, 03 2015. doi: 10.1088/2041-8205/804/1/L5.

Paola Matteo, M. Haywood, M. Lehnert, Dahlya Katz, S. Khoperskov, O. Snaith, A. Gómez, and N. Robichon. The milky way has no in-situ halo other than the heated thick disc. composition of the stellar halo and age-dating the last significant merger with gaia dr2 and apogee. *Astronomy & Astrophysics*, 632, 10 2019. doi: 10.1051/0004-6361/201834929.

Marshall McCall. A council of giants. *Monthly Notices of the Royal Astronomical Society*, 440, 03 2014. doi: 10.1093/mnras/stu199.

Alan McConnachie. The observed properties of dwarf galaxies in and around the local group. *AJ*, 144, 04 2012a. doi: 10.1088/0004-6256/144/1/4.

Alan McConnachie. The observed properties of dwarf galaxies in and around the local group. *AJ*, 144, 04 2012b. doi: 10.1088/0004-6256/144/1/4.

Dante Minniti, R. Saito, J. Alonso-García, P. Lucas, and Maren Hempel. The edge of the milky way stellar disk revealed using clump giant stars as distance indicators. *Astrophysical Journal Letters*, 733, 05 2011. doi: 10.1088/2041-8205/733/2/L43.

Grevesse Nicolas and Edward Anders. Solar-system abundances of the elements - a new table. 183, 02 1989. doi: 10.1063/1.38013.

Andrew Pontzen, Rok Roškar, Greg Stinson, and Rory Woods. pynbody: N-Body/SPH analysis for python. Astrophysics Source Code Library, record ascl:1305.002, May 2013.

Simon Pustilnik, Arina Tepliakova, and A. Kniazev. Study of galaxies in the lynx-cancer void. ii. element abundances. *Astrophys. Bull.*, 66, 08 2011. doi: 10.1134/S1990341311030011.

Jorge Sarrato. Unveiling the history of the milky way with a set of cosmological simulations from the hestia, magicc and nihao projects. *TFM, ULL*, 494, 2022.

Till Sawala, Marius Cautun, Carlos Frenk, John Helly, Jens Jasche, Adrian Jenkins, Peter Johansson, Guilhem Lavaux, Stuart McAlpine, and Matthieu Schaller. The milky way's plane of satellites is consistent with lcdm. *Nature Astronomy*, 7:1–11, 12 2022. doi: 10.1038/s41550-022-01856-z.

Frederic Schuller, J. Urquhart, T Csengeri, Dario Colombo, Ana Duarte-Cabral, Michael Mattern, Adam Ginsburg, A Pettitt, F Wyrowski, Loren Anderson, F Azagra, Peter Barnes, M Beltran, H Beuther, S Billington, L Bronfman, R Cesaroni, C Dobbs, David Eden, and M Wienen. The sedigism survey: First data release and overview of the galactic structure. *Monthly Notices of the Royal Astronomical Society*, 500, 09 2020. doi: 10.1093/mnras/staa2369.

Edward Shaya and R. Tully. The formation of the local group planes of galaxies. *Monthly Notices of the Royal Astronomical Society*, 436, 07 2013. doi: 10.1093/mnras/stt1714.

O. Snaith, M. Haywood, Paola Matteo, M. Lehnert, Francoise Combes, Dahlya Katz, and A. Gómez. Reconstructing the star formation history of the milky way disc(s) from chemical abundances. *Astronomy & Astrophysics*, 578, 10 2014. doi: 10.1051/0004-6361/201424281.

Volker Springel. E pur si muove: Galilean-invariant cosmological hydrodynamical simulations on a moving mesh. *Monthly Notices of the Royal Astronomical Society*, 401, 01 2009. doi: 10.1111/j.1365-2966.2009.15715.x.

Edouard Tollet, Andrea Macciò, Aaron Dutton, Greg Stinson, Liang Wang, Camilla Penzo, Thales Gutcke, Tobias Buck, Xi Kang, C. Brook, Arianna Di Cintio, Ben Keller, and James Wadsley. Nihao iv: Core creation and

destruction in dark matter density profiles across cosmic time. *Monthly Notices of the Royal Astronomical Society*, 456, 07 2015. doi: 10.1093/mnras/stv2856.

Laura Watkins, Roeland Marel, Sangmo Sohn, and Neil Evans. Evidence for an intermediate-mass milky way from gaia dr2 halo globular cluster motions. *The Astrophysical Journal*, 873:118, 03 2019. doi: 10.3847/1538-4357/ab089f.

Simone Weinmann, Frank van den Bosch, Xiaohu Yang, and H. Mo. Properties of galaxy groups in the sloan digital sky survey - i. the dependence of colour, star formation and morphology on halo mass. *MNRAS*, 366, 02 2006. doi: 10.1111/j.1365-2966.2005.09865.x.

Andrew Wetzel, Alis Deason, and Shea Garrison-Kimmel. Satellite dwarf galaxies in a hierarchical universe: Infall histories, group preprocessing, and reionization. *The Astrophysical Journal*, 807, 01 2015. doi: 10.1088/0004-637X/807/1/49.

Simon White and M. Rees. Core condensation in heavy halos - a two-stage theory for galaxy formation and clustering. *Monthly Notices of the Royal Astronomical Society*, 183:341–358, 04 1978. doi: 10.1093/mnras/183.3.341.

A Appendix

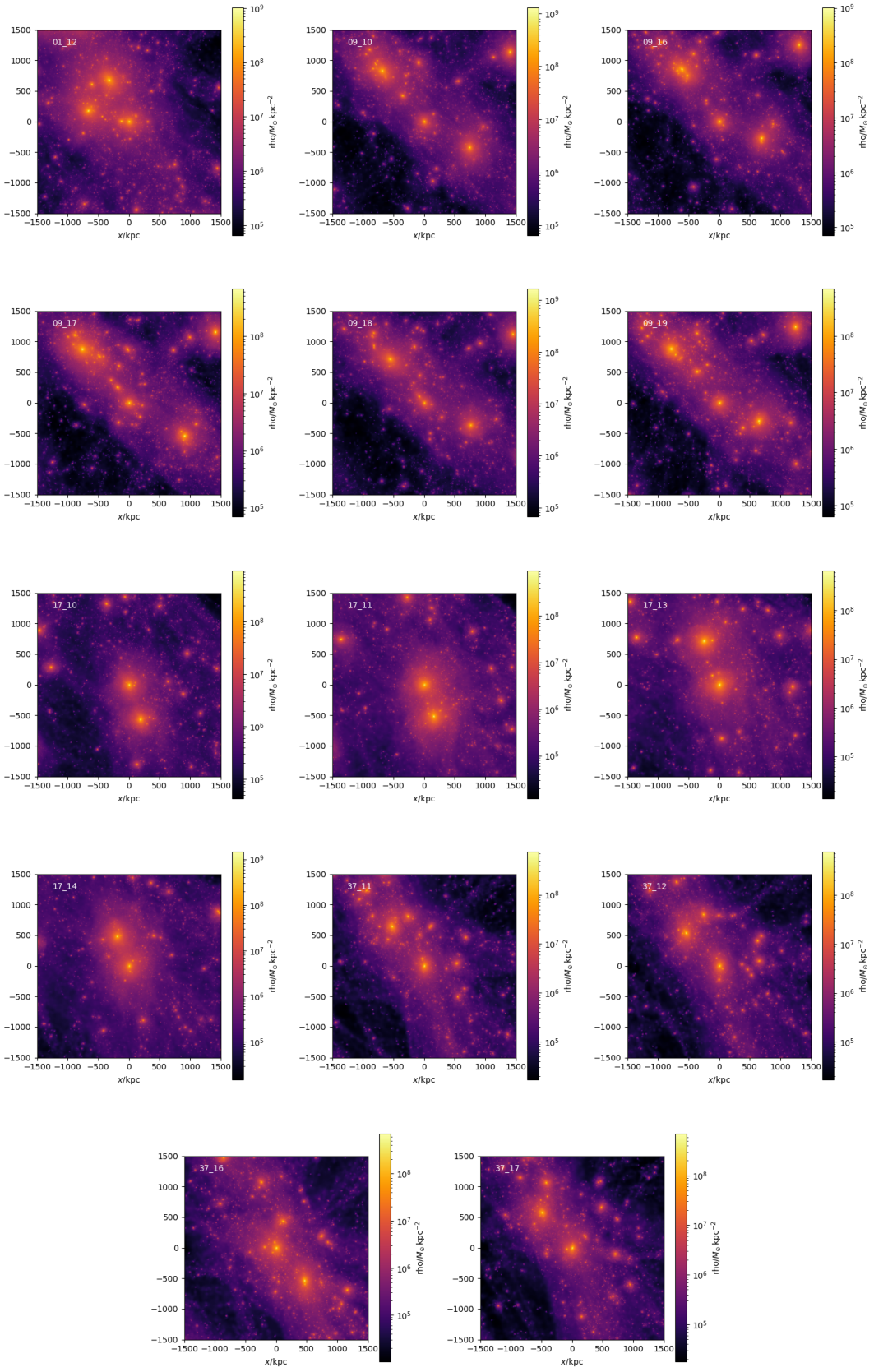

Figure 24: Dark matter distribution of the medium resolution local groups.

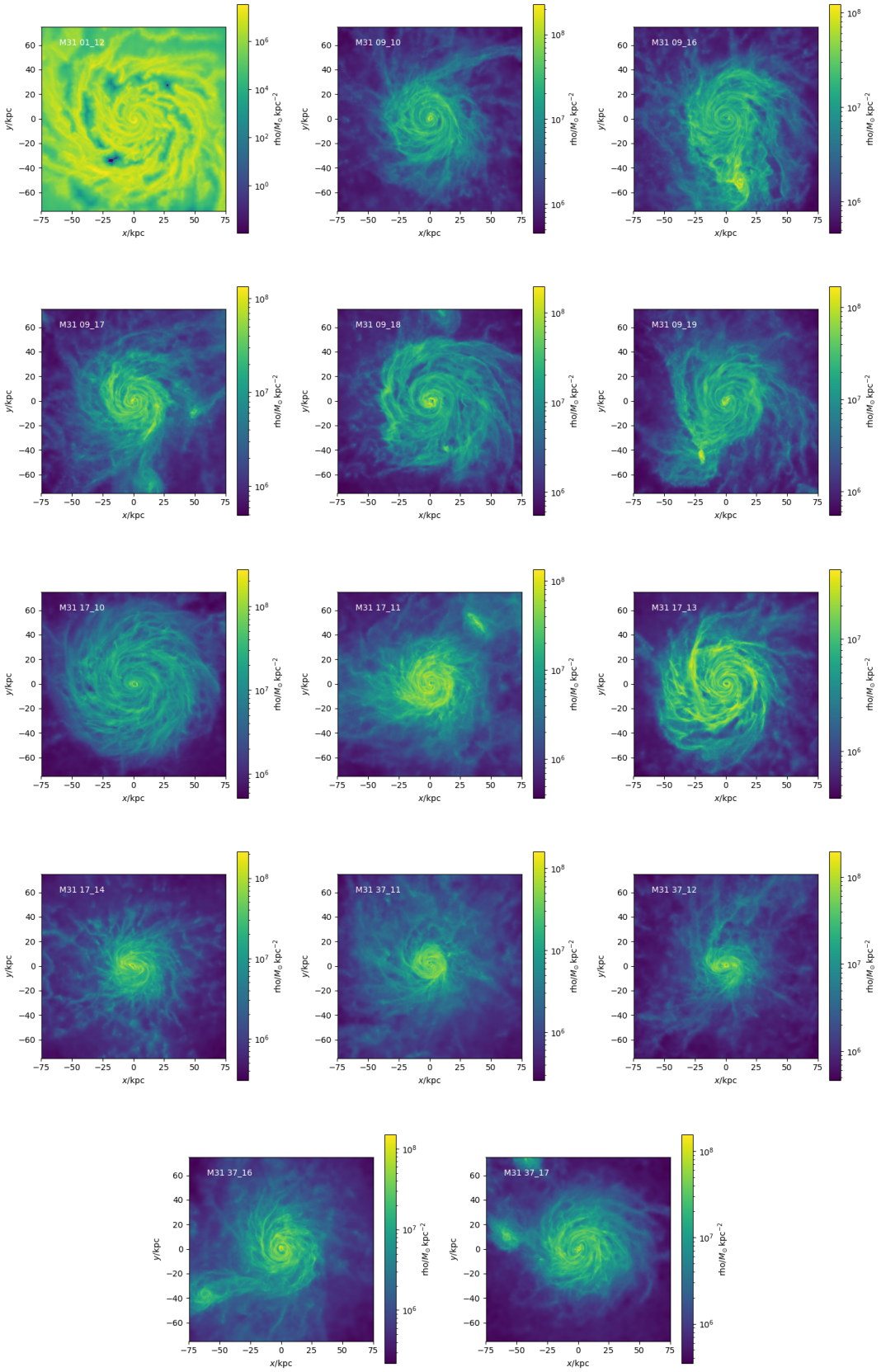

Figure 25: Face on gas distribution of the medium resolution M31 analogues.

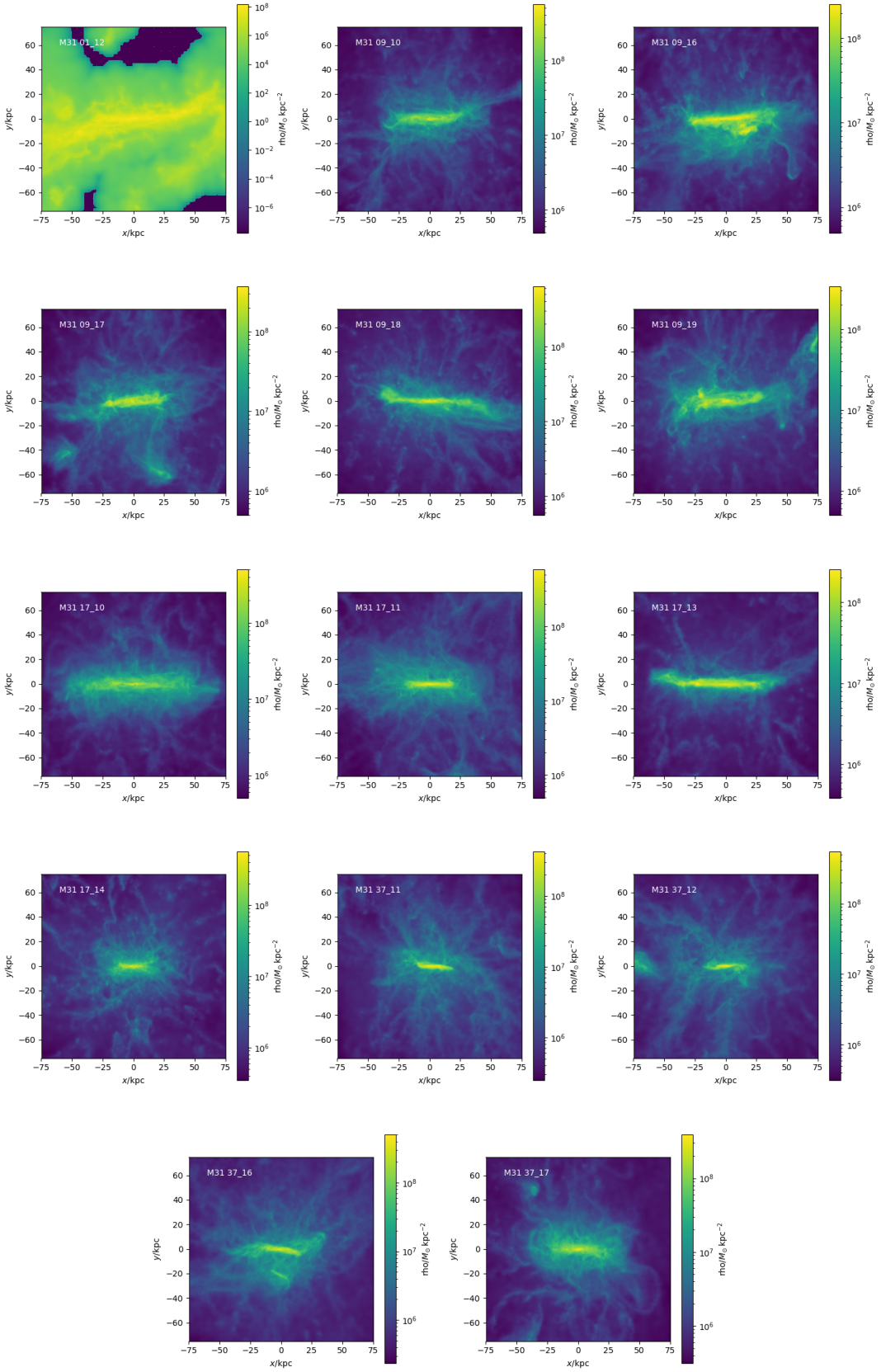

Figure 26: Edge on gas distribution of the medium resolution M31 analogues.

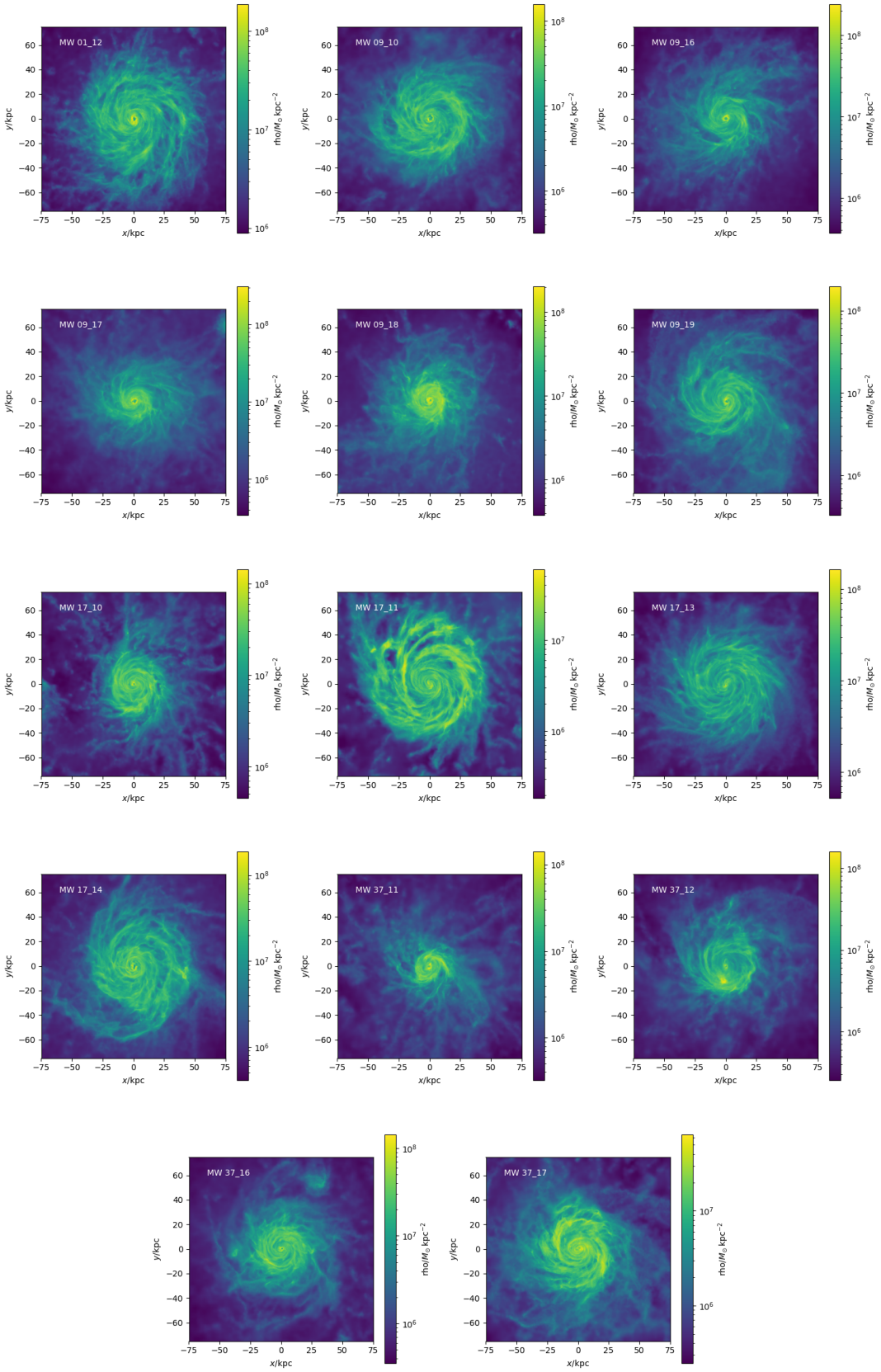

Figure 27: Face on gas distribution of the medium resolution MW analogues.

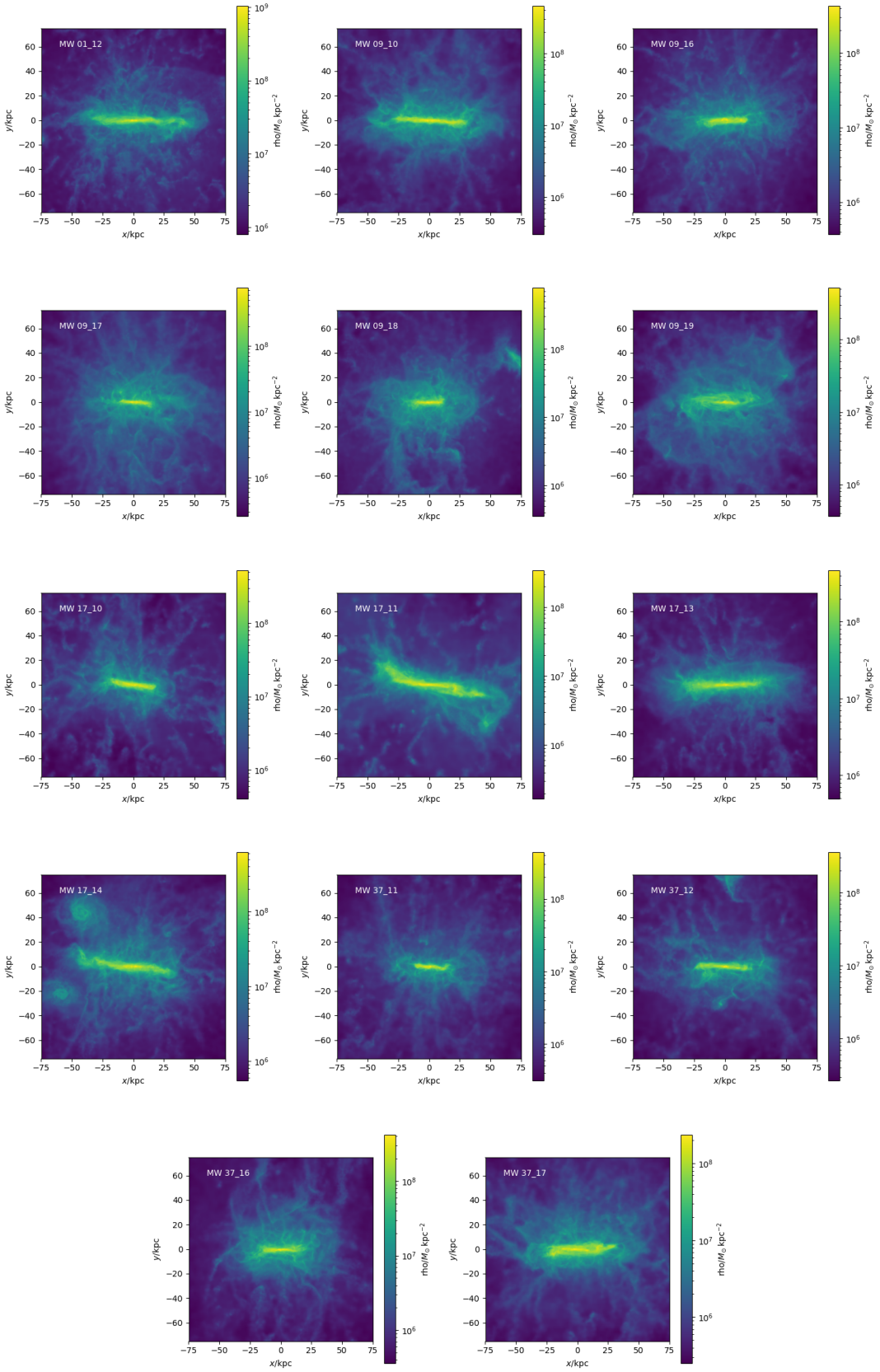

Figure 28: Edge on gas distribution of the medium resolution M31 analogues.

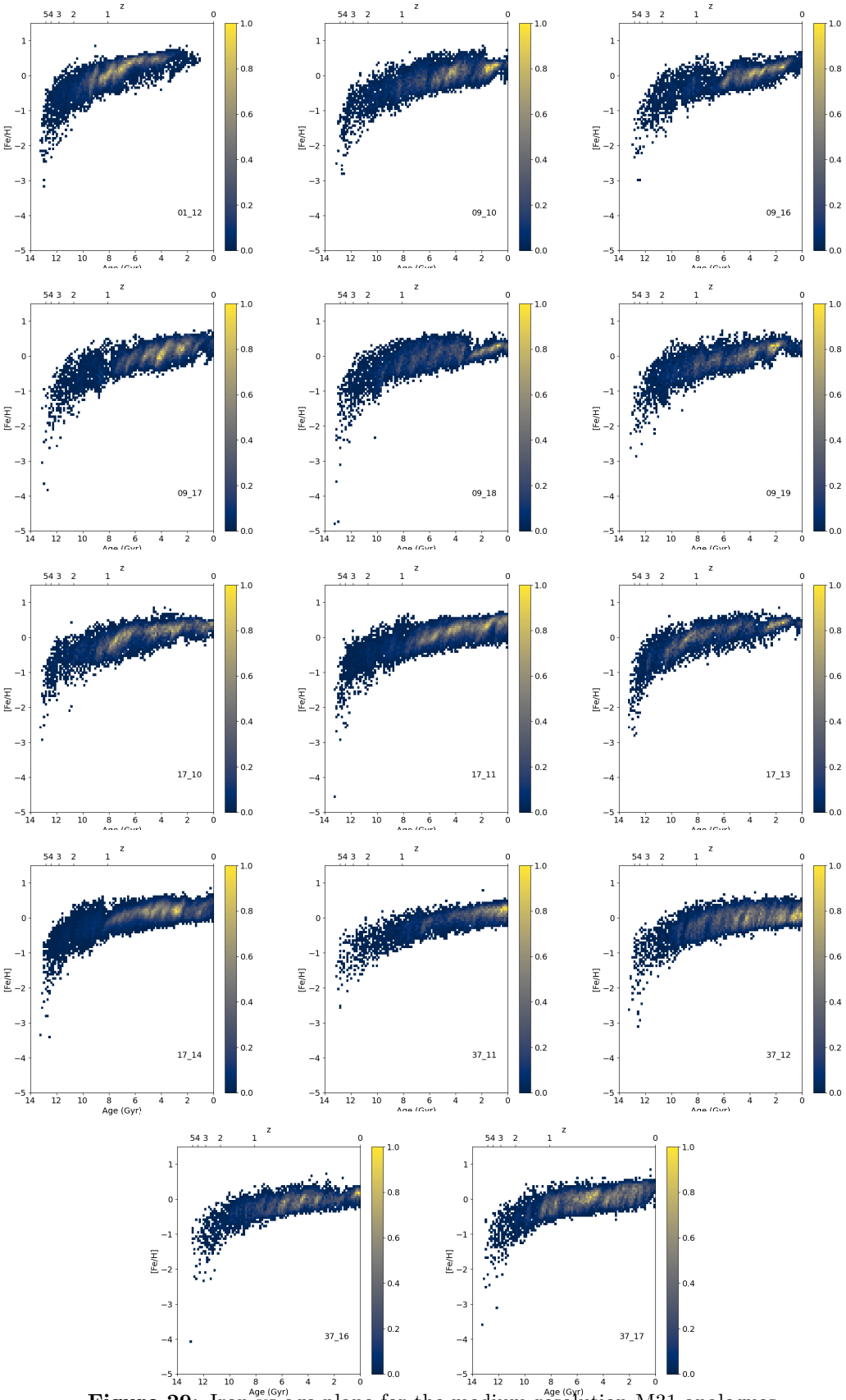

Figure 29: Iron vs age plane for the medium resolution M31 analogues.

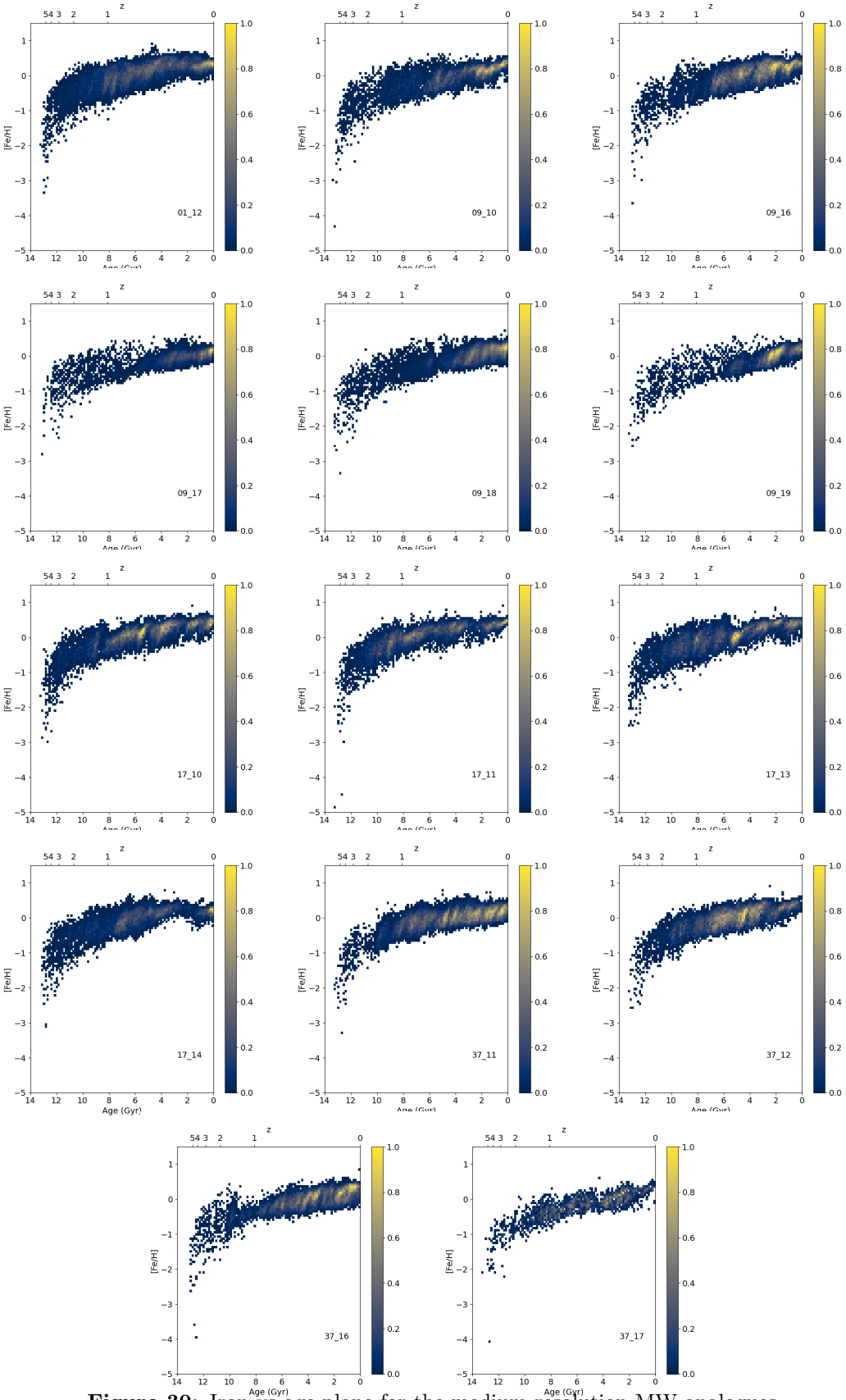

Figure 30: Iron vs age plane for the medium resolution MW analogues.

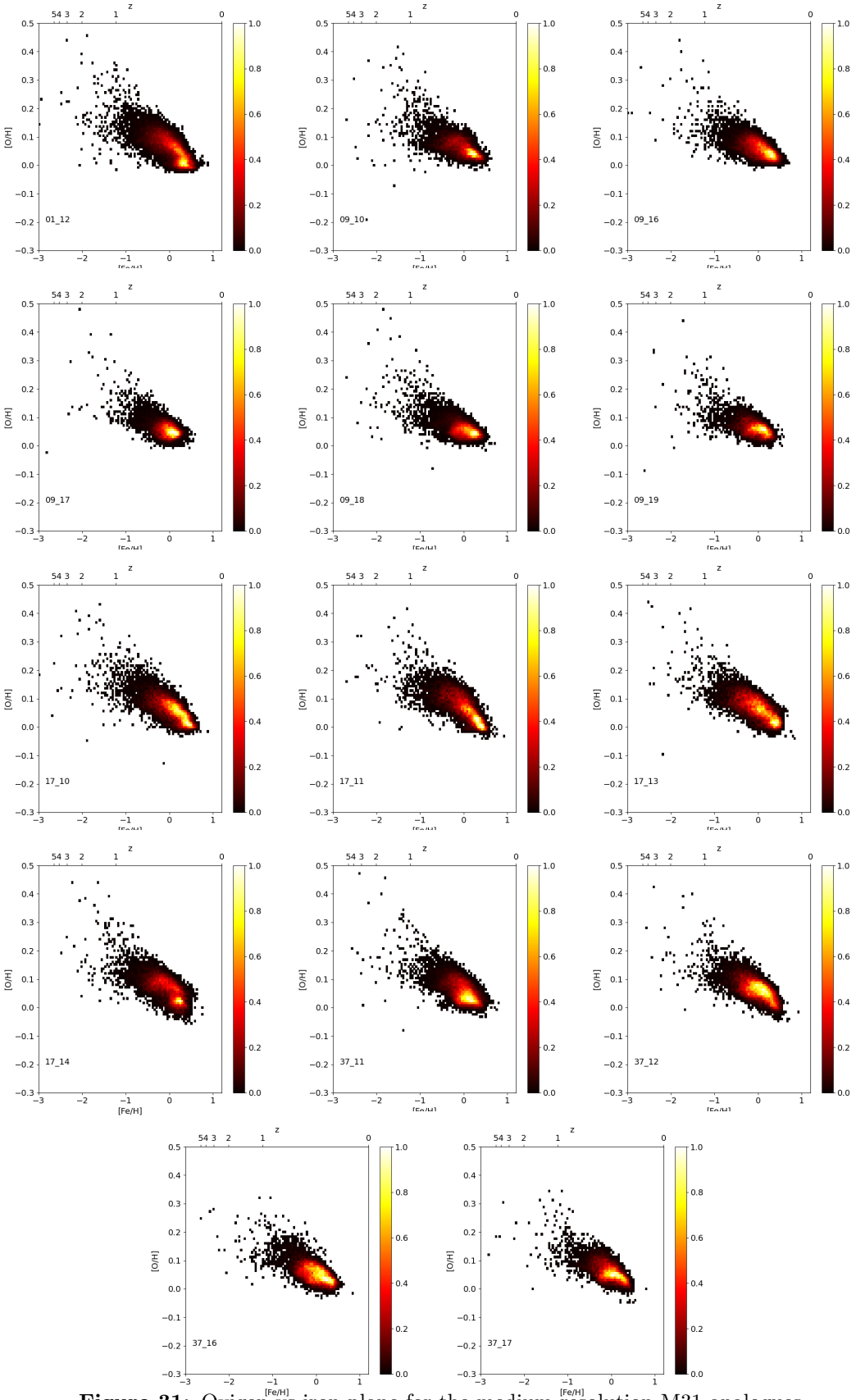

Figure 31: Oxigen vs iron plane for the medium resolution M31 analogues.

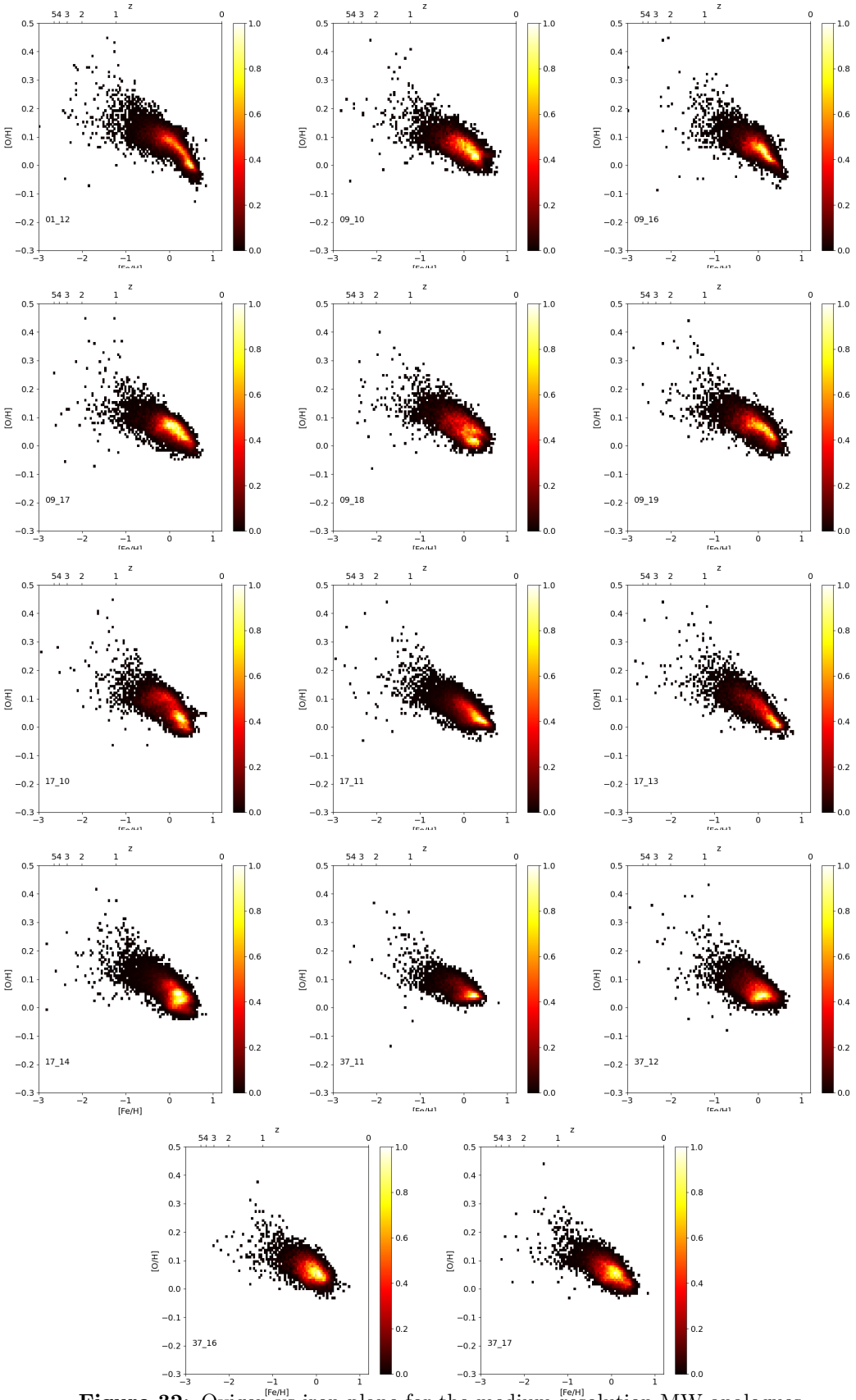

Figure 32: Oxigen vs iron plane for the medium resolution MW analogues.

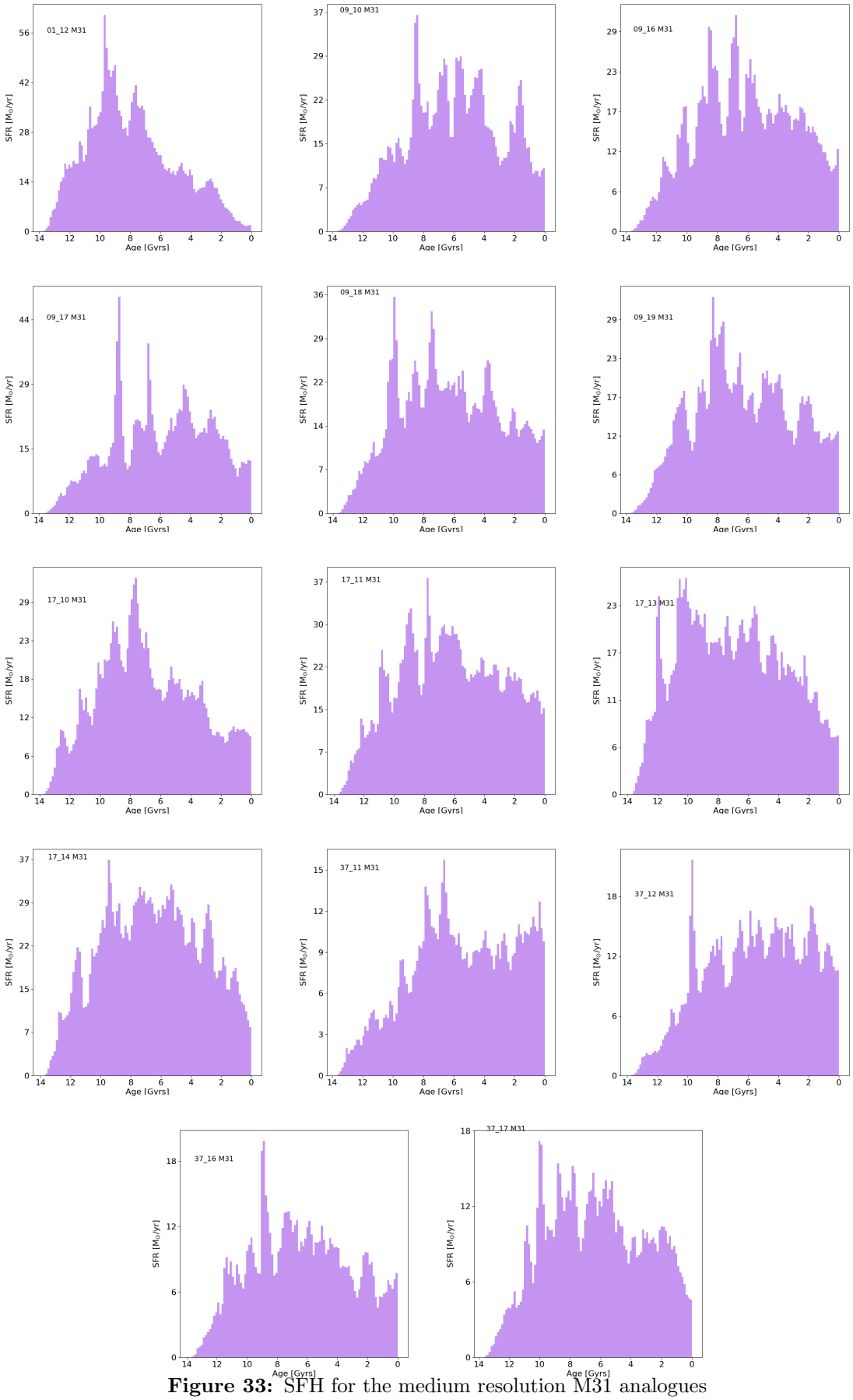

Figure 33: SFH for the medium resolution M31 analogues

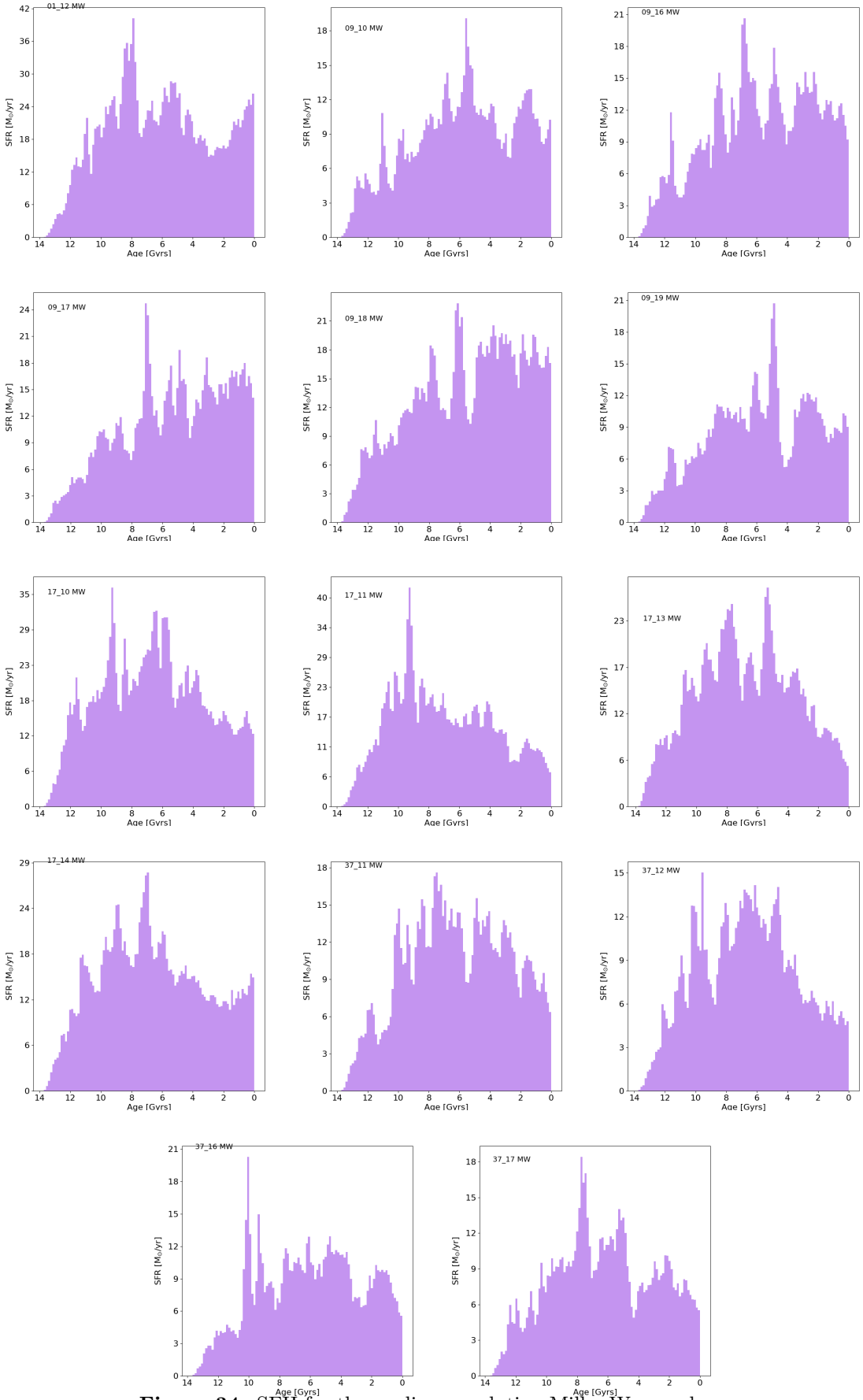

Figure 34: SFH for the medium resolution Milky Way analogues